Tectonics

RESEARCH ARTICLE
10.1029/2017TC004936

Special Section:
Geodynamics, Crustal and Lithospheric Tectonics, and active deformation in the Mediterranean Regions (A tribute to Prof. Renato Funiciello)

Evolution of the Ridges of Midelt-Errachidia Section in the High Atlas Revealed by Paleomagnetic Data

S. Torres-López[1], A. M. Casas[2], J. J. Villalaín[1], B. Moussaid[3], V. C. Ruiz Martínez[4], and H. El-Ouardi[5]

[1]Departamento de Física, Escuela Politécnica Superior, Universidad de Burgos, Burgos, Spain, [2]Geotransfer Research Group (IUCA), Universidad de Zaragoza, Zaragoza, Spain, [3]Département des sciences naturelles, Ecole Normale supérieure, Université Hassan II, Casablanca, Morocco, [4]Departamento de Geofísica y Meteorología, Facultad de Física, Universidad Complutense de Madrid, Madrid, Spain, [5]Département de Géologie, Faculté des Sciences, Université Moulay Ismail, Meknès, Morocco

Abstract New paleomagnetic data (43 sites) from Mesozoic sediments are contributed in this work, verifying the presence of a pervasive syntectonic Early Cretaceous remagnetization in the easternmost area of the Moroccan High Atlas. Using the small circle intersection method, we have calculated the characteristic remagnetization direction (Dec: 337.3, Inc: 38.4) that fits with a 100-Ma age, according to the Apparent Polar Wander Path of Africa. The paleomagnetic vectors of remagnetization are used to obtain the geometry during the remagnetization stage (100 Ma) of one of the most renowned geological cross sections of the High Atlas, the Midelt-Errachidia profile. The partial restoration of the cross section at 100 Ma allows us to determine the dips of the beds at the remagnetization stage in five structures (ridges or anticlines). Our results indicate that the five ridges that configure the Midelt-Errachidia profile were initiated to different degrees prior to wholesale compressive deformation during the Cenozoic. This configuration can be explained according to two different scenarios that we discuss in this paper: transpression and diapirism. The geological model obtained, both at present and at 100 Ma, indicates the existence of a Mesozoic cover substantially décolled from the Paleozoic basement, what strongly contrasts with previously published transects of the same area.

Key Points:
- A widespread Albian-Cenomanian remagnetization affecs the Mesozoic sediments of the Central High Atlas, Midelt-Errachidia cross section
- Restoration of syn-tectonic remagnetization allows obtaining the geometry of the basin at the age of the remagnetization
- We provide four detailed restored cross sections at 100 Ma considering two different scenarios, transpression, and diapirism

Correspondence to:
S. Torres-López,
storres@ubu.es

Citation:
Torres-López, S., Casas, A. M., Villalaín, J. J., Moussaid, B., Ruiz Martínez, V. C., & El-Ouardi, H. (2018). Evolution of the ridges of Midelt-Errachidia section in the High Atlas revealed by Paleomagnetic data. *Tectonics*, *37*. https://doi.org/10.1029/2017TC004936

Received 20 DEC 2017
Accepted 26 JUL 2018
Accepted article online 9 AUG 2018

1. Introduction

The main geodynamic stages affecting the High Atlas are well documented and basically consist of a Triassic-Early Jurassic extensional stage including two phases of rifting (Beauchamp et al., 1999; Frizon de Lamotte et al., 2000; Laville & Piqué, 1992) and a compressional stage during the Cenozoic which produced the inversion of the Mesozoic basins generated in the extensional stage (Arboleya et al., 2004; Michard et al., 2011; Teixell et al., 2003). However, there is a lack of information during the period of supposed tectonic quiescence covering the Late Jurassic and Early Cretaceous times.

This general geodynamic context is imprinted in the characteristics present in the area of this study, the classical Midelt-Errachidia cross section (Figure 1). The structures in this section consist of primarily narrow thrust anticlines with NE-SW to E-W directions separated by wide, gentle synclines. Structures such as overlapping faults, relay ramps, coalesced faults, accommodation zones, and polarity changes on faults, typical of oblique extensional tectonics, as well as harpoon, pop-up structures, and box folds, are common along the profile.

The study of syn-folding remagnetizations has become a tool for obtaining the relative age of the remagnetization with respect to tectonic processes by using the incremental fold test (Kent & Opdyke, 1985; Scotese & Van der Voo, 1983). In the last years, one more step has been taken with the development of a method that allows obtaining the geometry at the age of the remagnetization (Villalaín et al., 2003, 2016) from the study of syn-folding remagnetizations. This method has been used satisfactorily in several works in the Iberian plate (Casas et al., 2009; Soto et al., 2008, 2011) and in the Central High Atlas (Calvín, Casas-Sainz, et al., 2017; Torres-López et al., 2016).

In this paper we present a paleomagnetic study on sedimentary rocks from the Moroccan High Atlas that corroborates that the remagnetization recently described in this region (Calvín, Casas-Sainz, et al., 2017; Moussaid et al., 2015; Torres-López et al., 2014) extends to the easternmost part to the Central High Atlas.

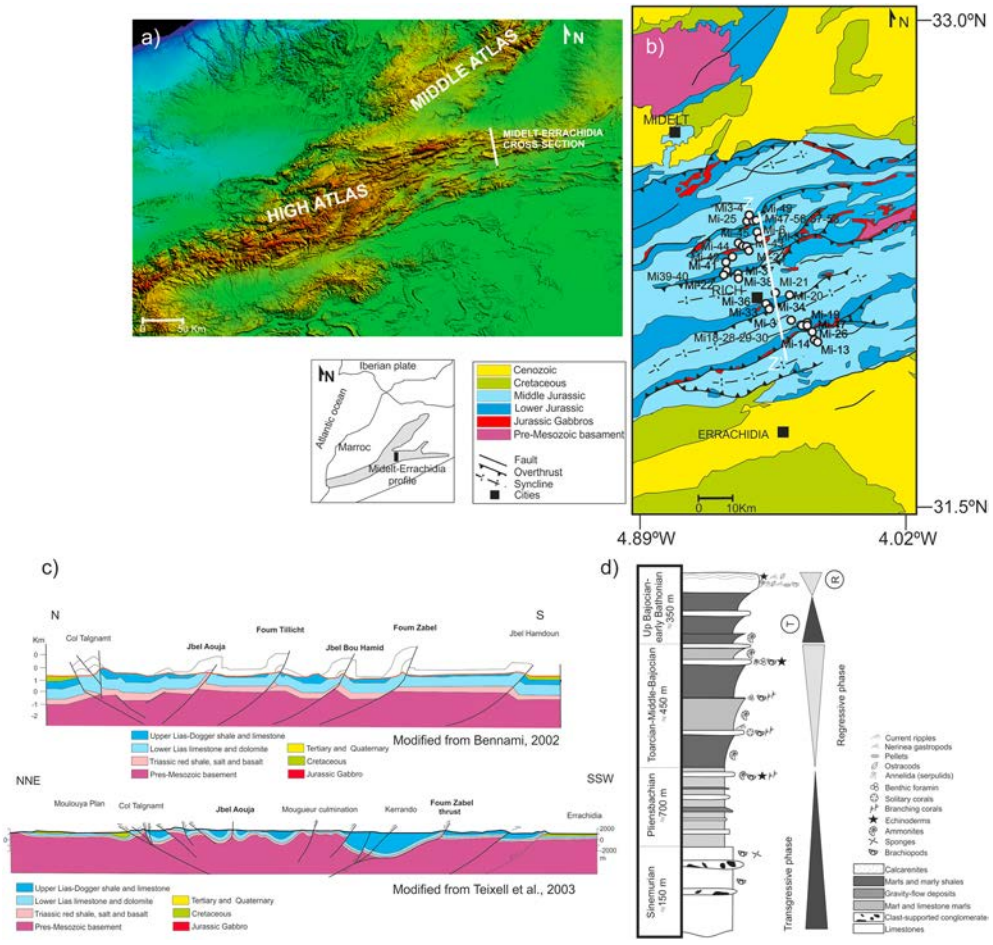

Figure 1. (a) Digital elevation model and geological sketch of the Central High Atlas and Midelt-Errachidia area. (b) Geological map of the Midelt-Errachidia area, showing the sample sites and the profile corresponding to figure. (c) Midelt-Errachidia cross sections modified from Benammi (2002) and Teixell et al. (2003). (d) Schematic stratigraphic column of the study area.

We apply the method of Villalaín et al. (2016) to obtain the geometry of the Midelt-Errachidia profile at the age of the remagnetization, at 100 Ma. This snapshot allows us to understand the relative chronology of structures and fold evolution. The results obtained are a contribution to the knowledge of the poorly known deformation processes occurred in the Central High Atlas during Late Jurassic and Early Cretaceous times.

2. Geology of the High Atlas

The Atlas is an intracontinental belt extending more than 2,000 km in North Africa. Two fold-and-thrust branches are distinguished in Morocco: the Middle Atlas, with NE-SW direction, and the High Atlas, with approximately E-W to ENE-WSW direction. The Atlas chains developed due to the inversion of the extensional or transtensional Mesozoic basins, as a consequence of the convergence between Africa and Europe during the Cenozoic (Jacobshagen et al., 1988; Laville & Piqué, 1992; Mattauer et al., 1977). The deformation occurred in the High Atlas is polyphased. During the Triassic, a rifting episode with NE-SW extension direction took place (Mattauer et al., 1977; Piqué et al., 2000). Successive extensional episodes are represented by red bed units with intercalated basaltic lava flows (Choubert & Faure-Muret, 1962) sedimented in graben structures. During the Jurassic, a second rifting formed basins elongated in NE-SW (Mattauer et al., 1977) and ENE-WSW (Laville & Piqué, 1992) directions. This second extensional stage is evidenced by lithostratigraphic changes which show bathymetric/environmental variations from deep to shallow water and lasted from the Early until the Middle Jurassic (Frizon de Lamotte et al., 2000). During the Early Jurassic, shallow marine

platforms, with increasing subsidence, controlled the deposition of carbonates. The Middle Jurassic was characterized by deposition of marl-limestone series, ending with a marine regression and the sedimentation of red bed deposits (Laville & Piqué, 1992). The convergence between Africa and Europe began at the end of the Mesozoic (Laville, 2002; Laville et al., 1977; Mattauer et al., 1977) but it is from the Eocene to present day when basin inversion and normal fault reactivation took place in the High Atlas (Bracène & Frizon de Lamotte, 2002; El Harfi et al., 2001, 2006; Frizon de Lamotte et al., 2008; Missenard, 2006). Compressional deformation is heterogeneously distributed: Deformation is concentrated in narrow anticlines or thrust faults of probable Cenozoic compressional origin, which are separated by broad synclines. Variations in Mesozoic stratigraphy and thickness of the Mesozoic series across thrust faults attest to their origin as syn-sedimentary extensional faults (Frizon de Lamotte et al., 2000). Jurassic sedimentary rocks crop out in the central and eastern segments of the Central High Atlas, being scarcer in the western part, where the Paleozoic outcrops abound.

The High Atlas underwent intense magmatic activity during the Triassic and throughout the Mesozoic, since alkaline transitional gabbroic magmatism continued during the Early Cretaceous and later times. The gabbroic bodies are located in the Central High Atlas specially (Bensalah et al., 2013; Zayane et al., 2002). Another remarkable feature in the Central High Atlas is the presence of Triassic evaporites and salt diapiric structures which appear in the core of several of the narrow anticlines known as ridges (French *rides*), a typical structure of this area. Most authors recognize the High Atlas as an extensive diapiric province (Saura et al., 2014, and references therein), attributing folding during the Jurassic basin-opening stage to salt diapirism of the Triassic layer (Michard et al., 2011; Saura et al., 2014; Teixell et al., 2017).

A phase of compressive folding and erosion, witnessed by unconformities and pervasive structures at the outcrop scale, was proposed for the Late Jurassic by Mattauer et al. (1972, 1977), Laville and Piqué (1992), and Laville et al. (2004). However, this compressional, intermediate stage is still controversial and not recognized by other authors (see e.g., Calvín, Casas-Sainz, et al., 2017; Frizon de Lamotte et al., 2008; Saura et al., 2014; Teixell et al., 2017).

Note that, in spite of the different interpretations of the tectonic structure in the two cross sections, especially regarding the elevation of the top of the basement and the homogeneity/heterogeneity in thickness of the Mesozoic series, both of them consider basement-driven compressional tectonics without significant décollements.

The stratigraphic series of the Midelt-Errachidia Jurassic profile begin with the Sinemurian platform carbonates (Figure 1) developed in the northern and southern basin borders and limestones and marly limestones with brachiopods, sponges, and crinoids toward the basin center. During the Late Sinemurian and Pliensbachian, deepening and individualization of the minibasins due to the second extensional stage occurred in the High Atlas, which generated new accommodation space and subsidence. The deposits are marls, limestones, and gravity-flow deposits corresponding to ramp-type to a shoal-rimmed morphology, while the basin deepened and the fault movement accelerated (Quiquerez et al., 2013; Wilmsen & Neuweiler, 2008). The Toarcian-Early Bajocian is characterized by a shallowing-upward cycle that begins with Toarcian marls and marly shales with ammonites and ends with shallow marine carbonate constructions and reefs (Ait Addi & Chafiki, 2013). This reflects increasing topography of the ridges and deepening of the depocenters in the central areas. The Bajocian-Early Bathonian is only preserved in the deepest synclines. It is formed by three units: The lowermost one consists of marls with ammonites intercalated with calcarenites; the second unit contains gray marls and nodular limestones and the upper unit shaly marls, nodular fine-grained limestones, and coral patch reefs with brachiopods, indicating a generalized regression.

The studied profile, the Midelt-Errachidia transect, is one of the best known of the Central High Atlas (Figure 1) and shows many of the common characteristics described for this area. The inverted Mesozoic sedimentary basin is at present limited by regional-scale thrusts in the northern and southern basin borders, with ENE-WSW directions. The Midelt-Errachida area shows narrow thrust anticlines with ENE-WSW trends separated by wide, gentle synclines. The tight anticlines are defined by Jurassic rocks: generally Liassic limestones crop out in the northern limb of the ridges and Dogger limestones in their southern limbs, whereas the synclines show Middle Jurassic materials in their cores and, more rarely, Triassic shales. Unlike the central part of the High Atlas, gabbroic bodies and salt walls are absent in the core of the ridges and the anticline hinges are faulted and sealed.

3. Paleomagnetic Methods and Sampling

A total of 51 sites, completing 464 cores, were sampled along a cross section with approximate N-S direction (about 45 km). The sampled series consist of black limestones, marly limestones, and marls, Early to Middle Jurassic in age, from Sinemurian to Bathonian. Black limestones belonging to Lias are strongly cemented, whereas marly limestones are less consolidated and show more ocher colors, typical of Dogger. The samples are distributed across the five ridges present in the profile (large-scale and metric-scale structures) and along the gentle synclines between ridges. Samples were taken by means of a gasoline portable drilling machine and oriented with a magnetic compass-inclinometer device. All paleomagnetic and rock magnetic analyses have been done in the Paleomagnetism Laboratory of the University of Burgos (Spain). The natural remanent magnetization of all specimens was routinely measured on a 2G-755 cryogenic magnetometer. After that, all specimens were subjected systematically to stepwise thermal demagnetization using a TD48-SC thermal demagnetizer in steps of 25° up to 550 °C. In addition, pilot samples, one or two for each station, were demagnetized using the alternating field technique. The steps for alternating field demagnetizing followed progressive peak fields, applying increasing fields of 2 to 10, 5 to 30, 10 to 60, and 20 to 100 mT. The characteristic magnetic component (ChRM) was isolated using linear regression techniques, and Fisher's (1953) statistics were used to compute the mean directions by using the Remasoft 3.0 software (Chadima & Hrouda, 2006).

For the purpose of analyzing the stability of the magnetic components, several fold tests in large-scale and metric-scale folds were performed. The statistical confidence of the fold tests was determined by the McFadden and Jones (1981) method. In order to know the properties of the carriers of the magnetization, several rock magnetic experiments were done. Representative samples were submitted to progressive acquisition of isothermal remanent magnetization (IRM) using a pulse magnetizer, reaching a maximum field of 2 T. Furthermore, samples were thermally demagnetized after they had acquired three orthogonal IRM components under fields of 2, 0.4, and 0.12 T (Lowrie, 1990). Thermomagnetic and backfield curves, as well as hysteresis loops, were performed by means of a Magnetic Variable Field Translation Balance.

3.1. Magnetic Properties

The thermal demagnetization reveals two stable components. One of them shows a maximum unblocking temperature of 250 °C and is usually aligned to the present-day magnetic field direction. This component is considered as a viscous magnetization and is not of interest for this work. After removing the viscous magnetization, a directionally stable, well-defined component presenting systematically normal polarity with unblocking temperatures comprised between 300° and 450 °C and intermediate coercivities between 20 and 100 mT (Figure 2 and Table 1) was observed.

The characteristics that define this component are the same as those described in the Imilchil area (100 km west of the Midelt-Errachidia section) by Torres-López et al. (2014) called component A in this work. Therefore, it has been identified as the remagnetized component observed in the Imilchil region (Calvín, Casas-Sainz, et al., 2017; Torres-López et al., 2014). A small variability in the maximum unblocking temperature (between 425 °C and 475 °C) is observed; nevertheless, the remagnetization component can be observed independently of the age and lithology.

The acquisition of IRM indicates that magnetization is saturated below fields of 0.4 T, suggesting that the dominant magnetic carriers have low coercivity (Figure 3). In the thermal demagnetization of three IRM components (Figure 3b), the low coercivity phase shows drops at unblocking temperatures between 425 and 525 °C, suggesting that fine grained magnetite is the main carrier. In some cases, this dominant magnetic phase coexists with a lower contribution of pyrrhotite (drop at about 320 °C in the intermediate phase), hematite, or rarely goethite (characteristic drops in the high coercivity phase). The thermomagnetic curves (Figure 3c) of some samples show very clear drops at 580 °C, what confirms the presence of magnetite observed in the IRM experiments (upper Figure 3a). In several samples, secondary magnetite and also probably pyrrhotite are generated during heating (lower Figure 3c). The parameters of hysteresis Mr/Mrs and Hcr/Hc (Figure 3d) of the samples are within the SD + SP mixture area (Dunlop, 2002) with approximate limits of $0.1 < Mrs/Ms < 0.5$ and $2 < Hcr/Hc < 20$. All in all, this grain size distribution is consistent with the unblocking temperatures observed in the thermal demagnetization of three orthogonal IRM, lower than the Curie temperature of magnetite.

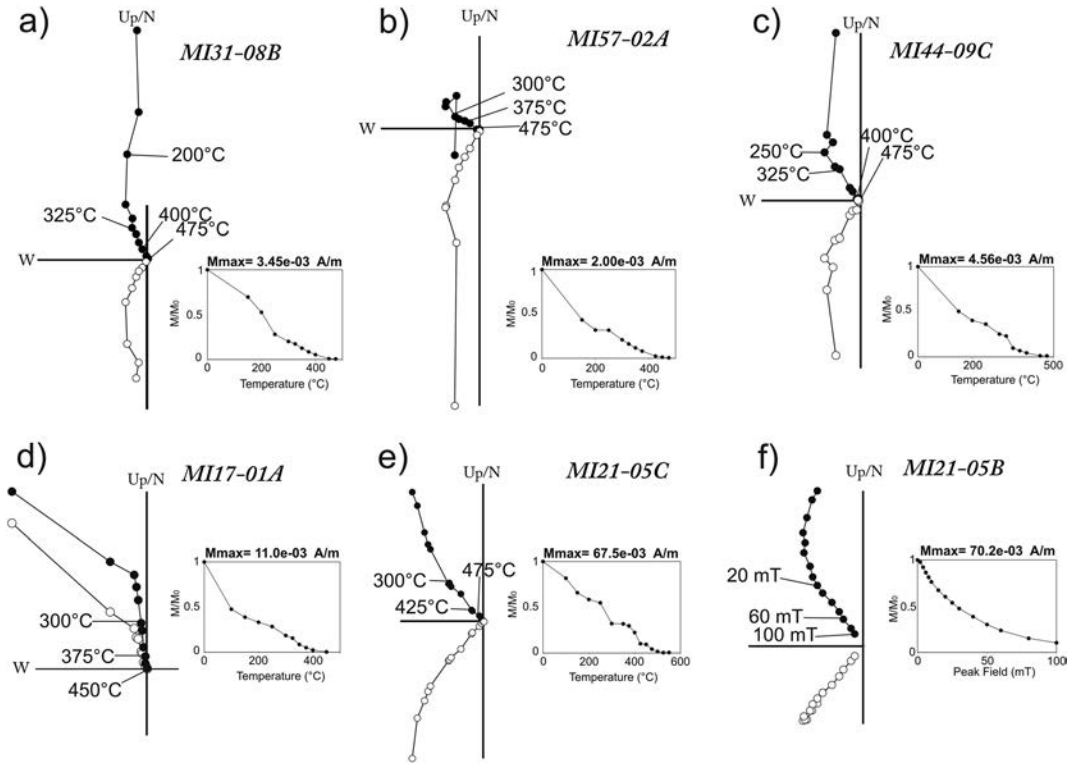

Figure 2. Natural remanent magnetization (NRM) (a–e) thermal and (f) alternating field demagnetizations of representative samples. All directions are plotted in in situ coordinates. The open symbols are projections of the vectors end points onto the vertical north-south plane, and the filled symbols are projections onto the horizontal plane. The evolution of normalized NRM intensity M/M_0 is shown in the insets.

4. Paleomagnetic Directions

The paleomagnetic directional analyses have been developed upon the ChRM described in the previous section which has been identified in 43 out of the 51 sites used in this study. The facts that (i) normal and reverse polarities appear frequently along the Jurassic and that (ii) ChRM systematically shows normal polarity suggest that it is a secondary magnetization or remagnetization. The mechanism of acquisition of remagnetization is probably chemical, according to the SD + SP mixture area (Jackson 1990; Channell & McCabe, 1994; Torres-López et al., 2014), as also inferred from studies in the sector of Imilchil (Torres-López et al., 2014).

A regional fold test using all site mean directions of the ChRM was performed (Figure 4). Site mean directions before and after bedding correction are scattered, indicating that the ChRM is a syn-tectonic remagnetization. It must be understood that a syn-tectonic remagnetization implies that the magnetization can be acquired either between subsequent tectonic stages separated in time and during the development of structures in a single event. To determine the relative age of the remagnetization in relation to specific structures, several fold tests were performed along the cross section in meter-scale and kilometer-scale folds.

The fold test performed in meter-scale folds (Figure 5a) shows that the paleomagnetic directions of the two flanks of the fold are clustered after the complete bedding correction, meaning that the remagnetization is in this case a predeformational event, with a clear prefolding acquisition at 95% level of confidence (McFadden & Jones, 1981). Figure 5b is an example of kilometer scale fold test: Sites 42 and 22 correspond to the northern and southern flanks of the syncline, respectively, between Sidi-Hamza and Foum-Tillich ridges. Paleomagnetic directions are scattered before and after bedding correction, suggesting an acquisition of remagnetization at an intermediate deformation stage. In the incremental fold test we observe that the maximum grouping takes place at an unfolding configuration of 35%, corresponding to a minimum f value (McFadden & Jones, 1981), indicating that both distributions present statistically the same direction at 95% level of confidence.

Tectonics

10.1029/2017TC004936

Table 1
Remanent Magnetization Parameters for the Characteristic Component

	Site	Age	Site coordinates		In situ Bedding	N/n	In situ				100% Tilt corrected		BFD corrected to D337° I38°		Restored bedding At 100 Ma		
			Lat (°)	Lon (°)	Dip dir, dip		α_{95}	*k*	*D*	*I*	*D*	*I*	*D*	*I*	φ	Dip dir	Dip
Jbel Aouja	MI-3	Upper Lias	32.458	4.499	315,29	8/8	6.8	67.2	350.0	50.0	338.9	24.5	342.6	37.2	17	315	12
	MI-4	Lower Lias	32.458	4.499	139,16	6/8	8.5	81.7	346.0	17.0	349.5	31.1	351.1	35.3	15	139	1
	MI-25	Lower Lias	32.453	4.497	334,35	8/8	2.4	539.1	357.0	53.0	348.5	19.7	351.2	37.2	19	334	16
	MI-49	Lower Lias	32.451	4.490	130,87	7/8	7.6	64.7	329.0	−22.0	345.7	58.9	333.0	39.4	66	130	21
	MI-48	Upper Lias	32.449	4.488	145,15	8/8	12.5	34.8	349.0	38.7	356.1	52.0	348.3	36.7	4	145	19
	MI-24	Lower Lias	32.443	4.487	330,76	6/8	10.8	37.6	15.0	75.0	340.6	3.2	343.4	37.9	42	330	34
	MI-47	Lower Lias	32.443	4.485	331,76	6/8	7.6	101.5	144.0	63.0	335.1	38.5	336.0	40.1	78	150	2
	MI-56	Lower Lias	32.444	4.485	356,13	7/8	7.7	75.7	350.0	61.0	351.7	48.1	352.2	39.9	19	176	6
	MI-57	Lower Lias	32.444	4.485	160,45	7/8	12.5	30.7	330.0	11.0	322.7	54.9	327.5	37.8	26	160	19
	MI-58	Lower Lias	32.444	4.485	328,75	6/9	12.0	31.8	156.0	69.0	324.5	35.8	324.3	38.7	72	328	3
	MI-6	Upper Lias	32.434	4.476	116,09	9/10	6.0	81.3	340.0	35.0	345.1	41.2	341.2	36.6	1	116	10
	MI-55	Upper Lias	32.431	4.477	172,24	8/9	34.8	71.5	38.7	12.5	358.1	55.9	356.4	39.3	9	172	15
Sidi hamza-Foum	MI-46	Upper Lias	32.409	4.531	168,9	7/8	11.0	48.2	336.0	41.0	333.9	49.8	336.5	38.3	3	168	12
Tillich	MI-45	Upper Lias	32.402	4.525	165,48	6/8	10.0	44.7	336.0	26.0	317.3	72.4	334.7	38.2	12	165	36
	MI-44	Dogger	32.399	4.515	120,12	6/8	3.0	494.7	324.0	37.0	328.9	47.8	325.9	41.9	9	120	3
	MI-43	Upper Lias	32.396	4.509	325,87	7/8	5.4	126.2	221.0	70.0	305.4	7.6	300.6	36.5	59	325	28
	MI-23	Lower Lias	32.389	4.504	128,41	7/8	8.3	53.5	340.0	25.0	5.8	55.4	344.5	36.2	10	128	31
	MI-42	Lower Lias	32.378	4.522	145,45	7/8	7.7	62.2	341.0	8.2	350.5	50.7	345.1	37.3	29	145	17
	MI-41	Upper Lias	32.334	4.507	330,49	7/8	9.5	41.2	8.0	67.0	345.0	21.8	347.6	37.3	35	330	14
	MI-39	Lower Lias	32.318	4.544	033,62	5/8	8.0	91.7	332.0	41.0	351.7	−0.9	336.4	37.8	6	33	56
	MI-40	Lower Lias	32.318	4.544	340,50	5/8	7.0	119.5	341.0	53.0	340.6	3.0	340.8	38.5	15	340	36
	MI-22	Lower Lias	32.323	4.549	348,65	8/9	3.7	225.4	332.0	49.0	337.2	−14.6	334.7	38.2	12	348	53
	MI-37	Dogger	32.319	4.544	165,61	8/8	11.1	26.0	338.0	−1.4	331.4	58.9	336.1	38.3	40	160	25
	MI-38	Dogger	32.310	4.545	002,22	7/8	4.2	211.4	325.0	48.0	334.5	29.3	331.7	37.0	15	002	7
Bou Hamid	MI-21	Upper Lias	32.260	4.393	000,16	9/10	3.4	236.4	315.0	47.2	324.1	34.8	324.0	34.8	22	180	12
	MI-20	Upper Lias	32.273	4.481	036,33	9/9	5.4	93.2	319.00	42.0	340.9	28.0	333.5	35.3	21	036	12
	MI-36	Upper Lias	32.245	4.489	000,25	6/8	8.0	70.8	322.00	40.4	330.1	19.1	324.8	35.1	12	000	13
	MI-34	Lower Lias	32.238	4.489	328,69	6/8	7.4	83.7	327.0	69.2	327.6	00	327.5	38.8	30	328	39
	MI-35	Lower Lias	32.238	4.489	275,08	7/8	10.3	81.9	344.0	12.1	323.3	53.1	352.3	20.6	24	335	47
	MI-33	Upper Lias	32.234	4.488	335,85	8/8	7.3	59.1	311.0	75.3	328.9	−8.7	327.3	38.2	38	095	16
	MI-32	Upper Lias	32.239	4.419	150,86	8/8	18.0	8.7	334.0	−61.0	332.1	24.9	332.5	38.6	100	320	115
Foum Zabel	MI-19	Upper Lias	32.419	4.366	296,12	10/10	3.4	236.4	315.0	47.0	333.7	47.1	329.6	41.3	17	116	5
	MI-18	Lower Lias	32.176	4.364	143,22	7/8	5.4	93.2	319.0	42.2	341.3	12.9	345.6	37.1	45	323	23
	MI-28	Lower Lias	32.176	4.364	345,69	6/8	8.0	70.8	322.0	40.2	352.0	−8.2	353.9	38.3	22	345	47
	MI-29	Lower Lias	32.176	4.364	337,22	5/8	7.4	83.7	327.0	69.0	343.8	−5.8	345.6	38.1	22	337	44
	MI-30	Lower Lias	32.176	4.364	344,60	6/8	10.3	81.9	344.0	12.3	343.4	−4.0	343.3	38.6	17	344	43
	MI-17	Lower Lias	32.173	4.535	358,68	10/10	7.3	59.1	311.0	75.1	348.6	−23.1	346.8	39.8	2	358	66
	MI-26	Dogger	32.167	4.367	135,21	6/8	18.0	8.7	334.0	−61.4	346.9	43.5	343.6	37.0	11	135	110
	MI-14	Upper Lias	32.119	4.362	030,5	7/8	17.0	14.0	350.0	41.6	352.5	37.1	347.6	44.0	9	210	114
	MI-13	Upper Lias	32.073	4.388	343,18	9/10	6.2	70.4	327.0	64.5	332.9	46.4	334.2	38.2	27	163	9
Other sites	MI-53	Upper Lias	32.526	4.512	308,52	9/10	7.6	54.0	297.0	34.0	304.7	22.2	303.9	42.2			
	MI-54	Upper Lias	32.498	4.492	140,40	9/9	13.2	21.7	336.0	34.0	2.3	70.2	337	38.5			

Note. N/n: number of sample directions used in the analysis versus number of demagnetized samples. k and α95: Fisher statistical parameters. D and I: Declination and Inclination of the characteristic magnetic component. BFD: Best fit direction. ϕ: Unfolding angle for restoration to the paleofield direction.

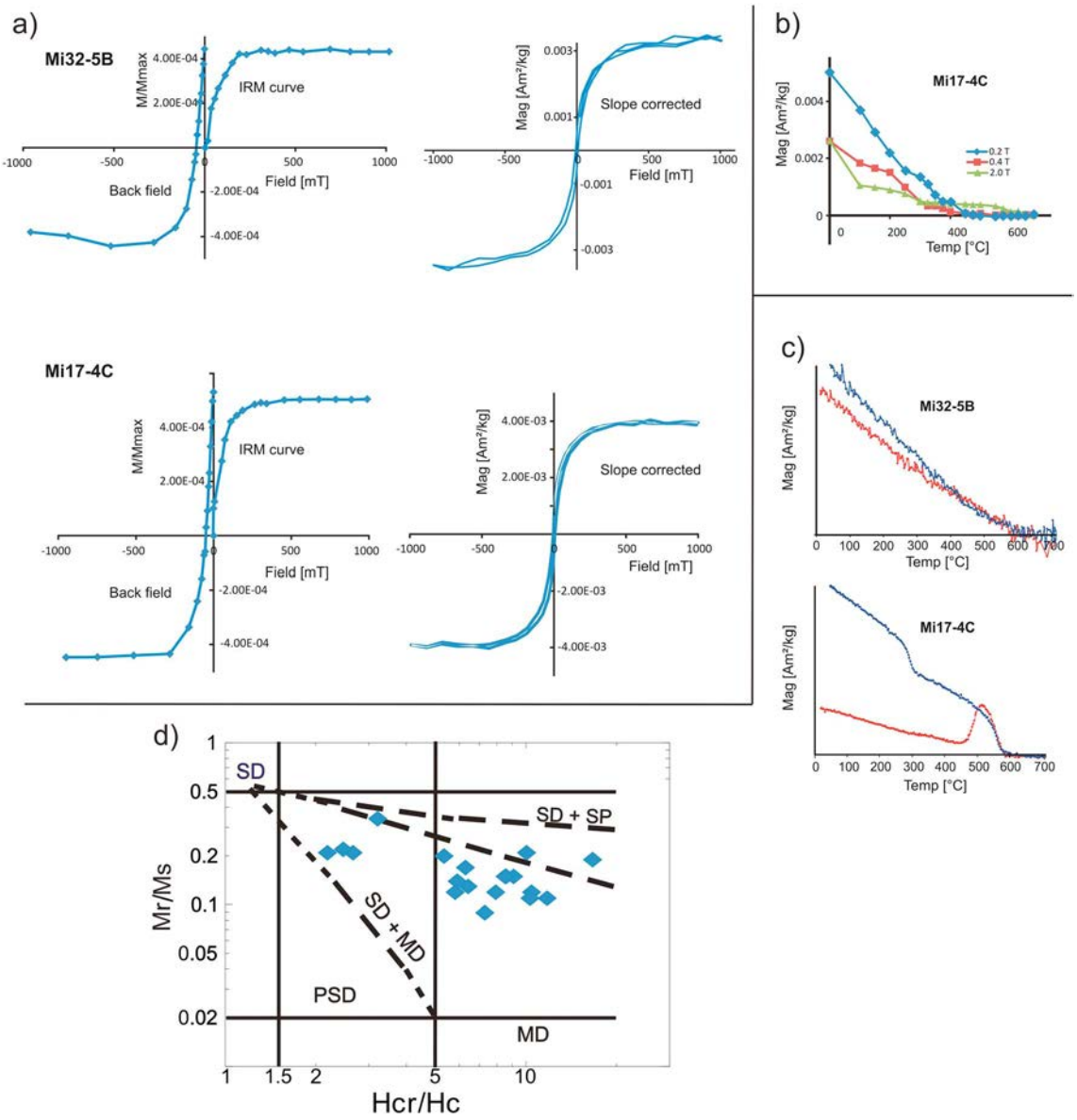

Figure 3. (a) Isothermal remanent magnetization (IRM) acquisition, back-field, and hysteresis loops after slope correction of representative samples. (b) Thermal demagnetization of three orthogonal IRM components of a representative sample. (c) Thermomagnetic curves of induced magnetization of representative samples. (d) Day diagram (Day et al., 1977), showing the hysteresis parameters for representative samples. SD, single domain; PSD, pseudosingle domain; MD, multidomain; SP, superparamagnetic. The dashed lines indicate the theoretical reference lines following Dunlop (2002) for SD + SP and SD + MD.

The two different responses to the fold test found in folds of different scales indicate a different relative timing folding/remagnetization acquisition for both types and can be related to the tectonic evolution in the area. This will be discussed in the next sections, after defining the expected direction for the remagnetization vector.

5. Calculation of Remagnetization Direction and Age of the Remagnetization

Intersections of remanence small circles (SCs) are increasingly used in paleomagnetism to determine the paleofield direction from syn-folding remanences. This method was proposed by Shipunov (1997) and modified by Waldhör and Appel (2006). Remanences are often syn-folding and have been acquired at an intermediate stage of folding and then tilted further. The aim of the SCI (SC intersection) method is to know the characteristic direction of the remagnetization, assuming that (1) all sites were remagnetized at the

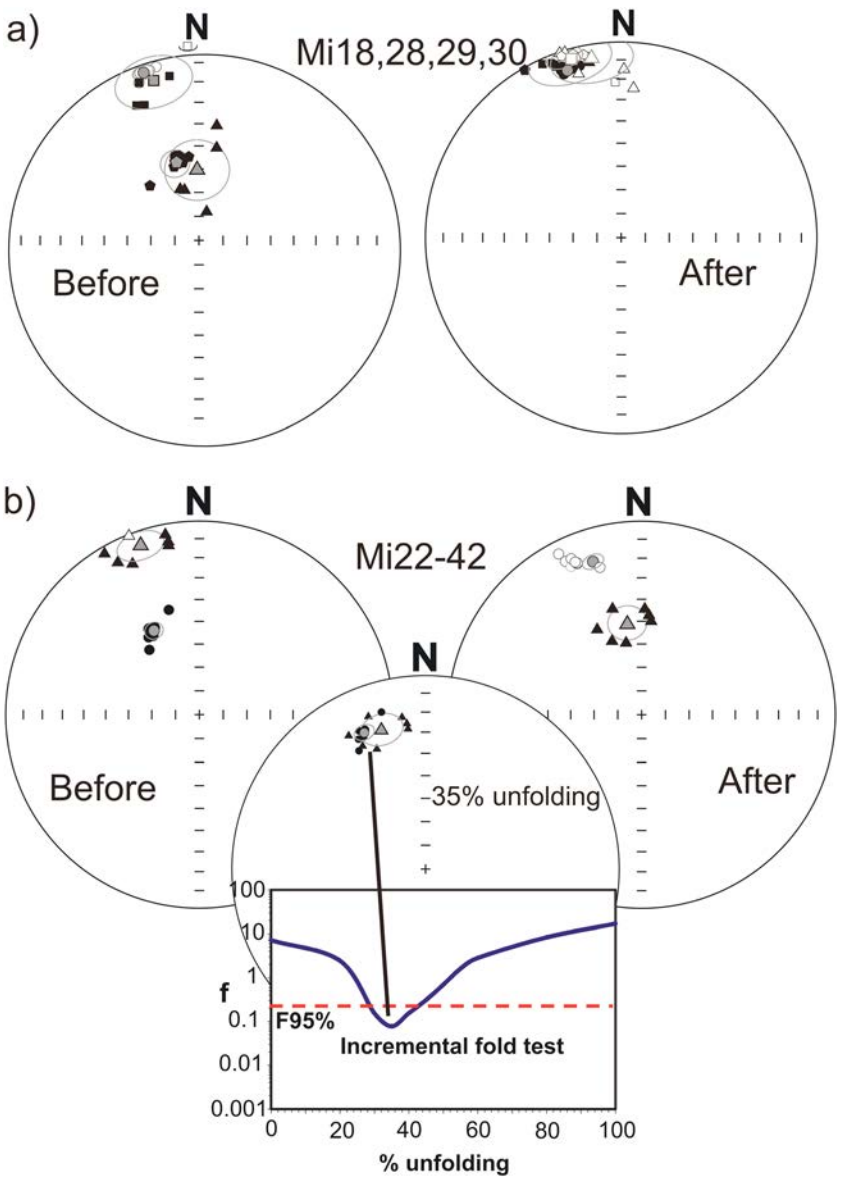

Figure 4. Equal-area projections showing directions for characteristic magnetization obtained in all samples before and after bedding correction. Mean direction and 95% confidence circles are also represented for each site. The filled symbols are plotted on lower hemisphere and open symbols on upper hemisphere.

same time and (2) during tilting, the direction of magnetization rotates around the strike of bedding and then the magnetization vector follows an SC trajectory centered in the bedding strike. The intersection of the SCs from different sites represents the single possible common magnetization direction (Shipunov, 1997), which can be interpreted as the characteristic direction of remagnetization.

The SCI solution has been calculated from 42 sites using the pySCu software (Calvín, Villalaín, et al., 2017): N: 43, Dec: 337.3, Inc: 38.4, η: 13.0, ξ: 3.5, A/n: 7.7° (Figures 6a and 6b). The remagnetization direction is given with a 95% uncertainty ellipse (Kent, 1982) obtained from a population of 500 solutions beginning with a parametric bootstrap allowing propagation of errors of the in situ paleomagnetic directions and bedding (Calvín, Villalaín, et al., 2017).

For the method to be successful, two premises have to be honored: (a) Between the sites, no differential rotations around vertical axes or other rotations around axes not parallel to bedding strike must have occurred and (b) the SCs have to intersect, which is an indicator of the quality of the result (Waldhör & Appel, 2006).

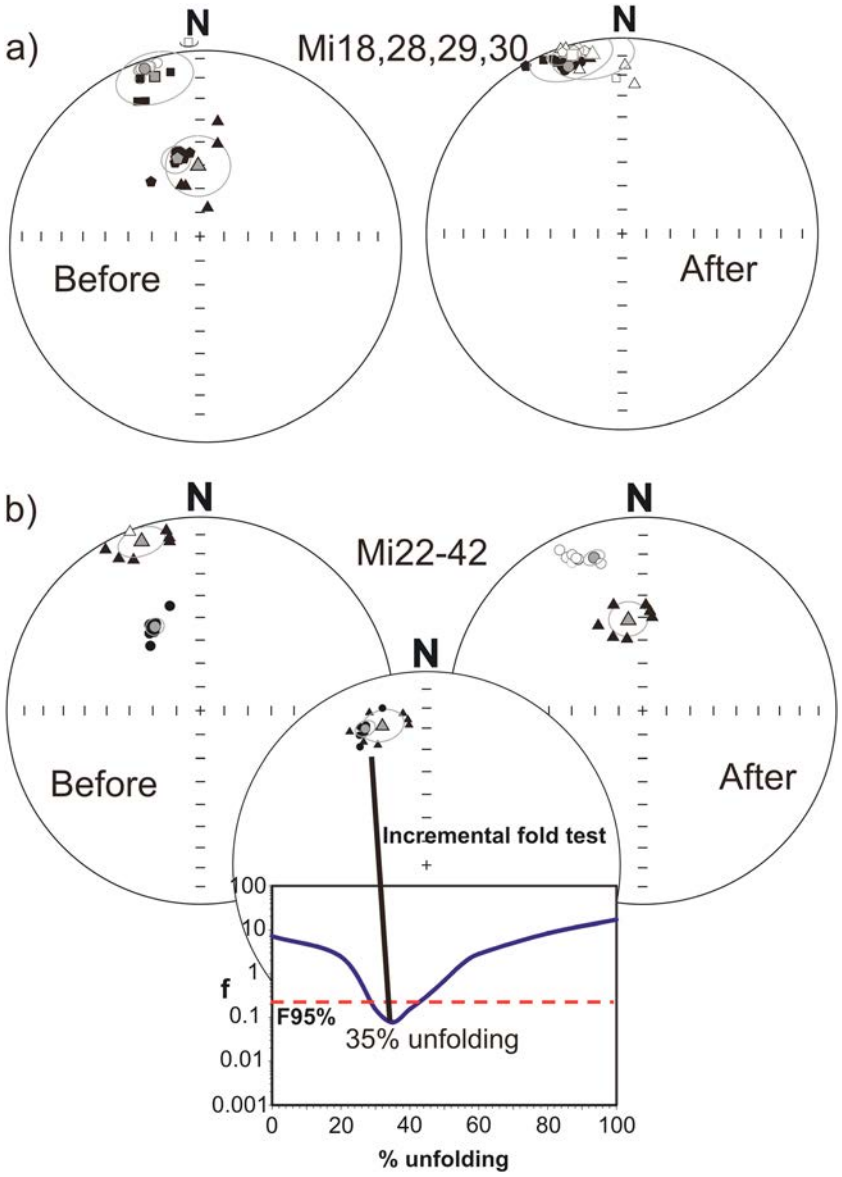

Figure 5. (A) Fold test in a meter-scale fold. The squares, pentagons, small circles, and triangles are directions corresponding to samples from different limbs before and after bedding correction (BC). Mean directions and 95% confidence circles are also shown. (b) Incremental fold test in a kilometer-scale fold. The small circles and triangles are directions corresponding to both limbs before and after BC and to the 35% unfolding. Mean direction and 95% confidence circle are also shown. Parameter f (McFadden & Jones, 1981) as a function of the percentage of unfolding of bedding tilt is represented in the graph. The horizontal dashed line represents the critical value of f at the 95% confidence level (F95%).

In the High Atlas there is no evidence of differential rotations around vertical axes between different parts of the chain (Teixell et al., 2003). Structures are generally coaxial (no complex tectonic histories), and there are no large block rotations between the High Atlas and the rest of the African plate, accordingly with its intracratonic character, the absence of large-scale changes of displacement along-strike of the main thrusts in the northern and southern borders of the High Atlas, and the existing paleogeographical reconstructions of the atlasic basin (Sibuet et al., 2012).

The bedding strike and the paleomagnetic direction define the shape of the SCs. Sites showing high errors in bedding strikes (dip $< 15°$) or high errors in paleomagnetic directions ($\alpha_{95} > 15°$) were removed from the calculation of the remagnetization direction.

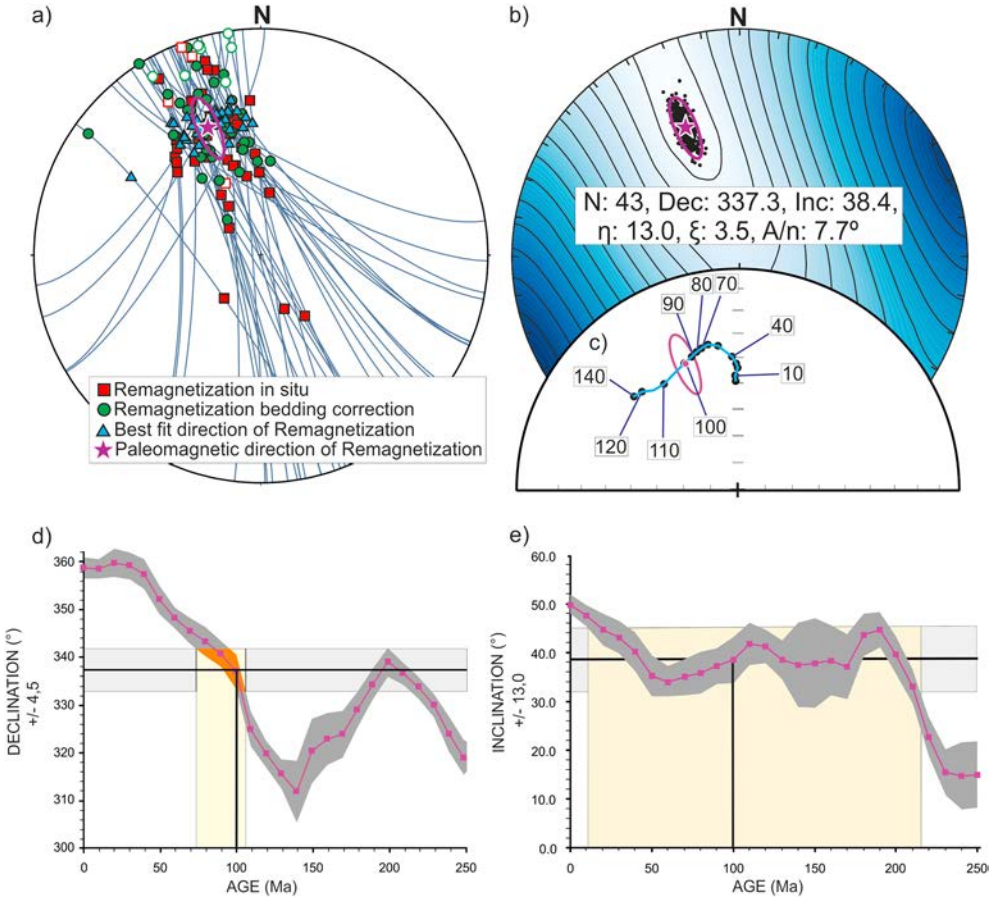

Figure 6. (a) Small circles corresponding to remagnetization directions from selected sites. The squares are mean directions of the in situ remagnetization for each site. The circles show the directions after bedding correction of the remagnetization. The triangles are the best fit directions of the remagnetization. The star shows the small circle intersection (SCI) solution, that is, the paleomagnetic direction of the remagnetization. (b) Equal area projections showing contours of equal value of A/n (Calvín, Villalaín, et al., 2017). The star shows the remagnetization solution for a population of 500 solutions (Calvín, Villalaín, et al., 2017). The 95% confidence ellipse is also shown. (c) The curve shows the expected paleomagnetic directions at the Central High Atlas from the Global Apparent Polar Wander Path (GAPWP) in African coordinates (Torsvik et al., 2012) as well as the SCI solution and its confidence ellipse. (d and e) Declination and inclination-age curves, expected in the Central High Atlas from the GAPWP in African coordinates (Torsvik et al., 2012). Uncertainties of the expected direction are shown. The horizontal line represents the observed declinations/inclinations and their uncertainties. The vertical shaded region indicates possible solutions.

The obtained direction for the remagnetization can be compared with the expected directions at the studied region obtained from the Global Apparent Polar Wander Path (GAPWP) in NW African coordinates (Torsvik et al., 2012). Figure 6d shows a broad solution in the inclination curve, ranging from 20 Ma up to 220 Ma (no specific solution). Conversely, the declinations curve points out a clear result at the age of about 100 Ma (Figure 5c) coinciding with the age calculated for the remagnetization in previous works (Calvín, Casas-Sainz, et al., 2017; Moussaid et al., 2015; Torres-López et al., 2014). The direction obtained is completely coincident with the direction from GAPWP at 100 Ma (Figure 6c). The uncertainty in the inclination can be explained by coaxiality of structures that cause the arrangement of the SCs intersections along a narrow, elongated band (Figures 6a and 6b) that constrains the value of the declination but gives a large error in the inclination value. On the other hand, the shape and distribution of the SCs depends on the angle between the strike of bedding and the remagnetization direction. In the case of the Central High Atlas, the direction of the remagnetization is practically perpendicular to the strike; this fact contributes to elongate intersection area in inclination giving a narrow uncertainty in declination. The fact that the High Atlas did not vary in latitude during the Mesozoic is also a cause of uncertainty in age determination when only using the inclination

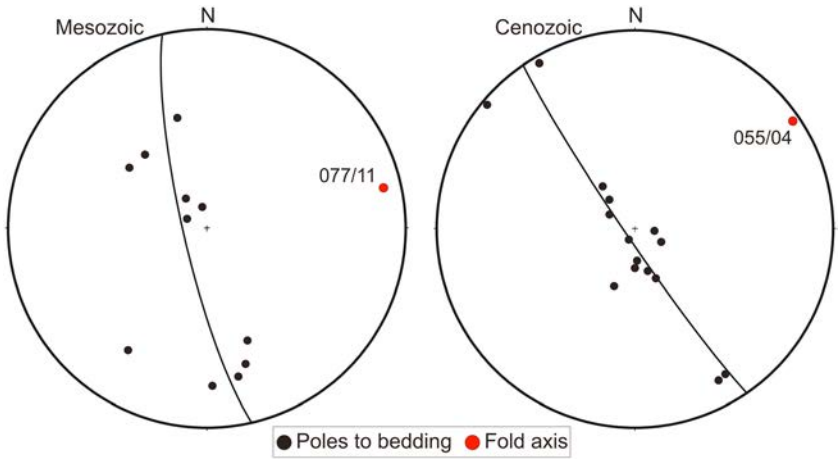

Figure 7. Equal area projections showing the poles of bedding of the rich area mostly acquired during the pre-Cenozoic (unfolding angle for restoration to the paleofield direction <30% of the present-day bedding) and during the Cenozoic (>70% of the present-day bedding) stages. The fold directions obtained are also shown.

of the remagnetization direction. The uncertainty ellipse obtained intersects the curve of expected directions from the GAPWP (Torsvik et al., 2012) in a well-defined direction corresponding to 100 Ma (D = 337.3, I = 38.4°), being both directions statistically indistinguishable (Figure 6c).

6. Reconstruction Methodology

We applied the method developed by Villalaín et al. (2003, 2016) that allows determining the geometry of folds in an intermediate deformation stage. The difference with respect to other techniques such as the incremental fold test, for the study of remagnetizations, is the assumption of nonsymmetric deformational histories. This issue is especially interesting when the remagnetization has been acquired between two different tectonic events. Therefore, the attitude of strata at the moment of the remagnetization is not necessarily horizontal, since there is a previous deformational event that conditions the geometry at the time of acquisition and its subsequent deformation due to a second tectonic event. Remagnetizations acquired before tectonic inversion of the basins but after syn-sedimentary deformation are relatively common (Calvín, Casas-Sainz, et al., 2017; Casas et al., 2009; Soto et al., 2008; Soto et al., 2011; Torres-López et al., 2016; Villalaín et al., 2003) because remagnetizations occur in sedimentary basins owing to different mechanisms during burial (Aubourg et al., 2012; Katz et al., 1998; Torres-López et al., 2014).

Starting from the expected direction of remagnetization obtained by means of the SCI method, the reconstructed geometry is obtained restoring bedding orientation to the remagnetization stage (paleodips) by rotating the magnetic directions of each site around the strike of bedding until the paleomagnetic mean vector reaches (or approaches as much as possible) the expected direction (Table 1). Each site will undergo the necessary rotation until reaching the expected direction, so that each limb of the same fold can undergo different amounts of rotation (Villalaín et al., 2016).

The only necessary hypothesis to be accomplished for the application of this method is that the different phases of folding should be broadly coaxial (Villalaín et al., 2016). In the High Atlas the faults developed during the extensional stage generated a strong anisotropy that conditioned the Cenozoic deformation, thus favoring coaxiality of fold axes. In addition, the SC analysis also allows to distinguish the structures mostly preremagnetization from post remagnezation (Figure 7). In the Midelt-Errachidia transect, poles to bedding for folds formed during the pre- and postremagnetization stages show axes forming a small angle (<20°), thus indicating that the two deformation stages were broadly coaxial. Another argument supporting this coaxiality is that, when restoring paleomagnetic data, an elongation of the distribution of possible solutions occurs along the SC (Figure 5), generating uncertainty in the calculation of the paleofield direction by the SCI method (Villalaín et al., 2016).

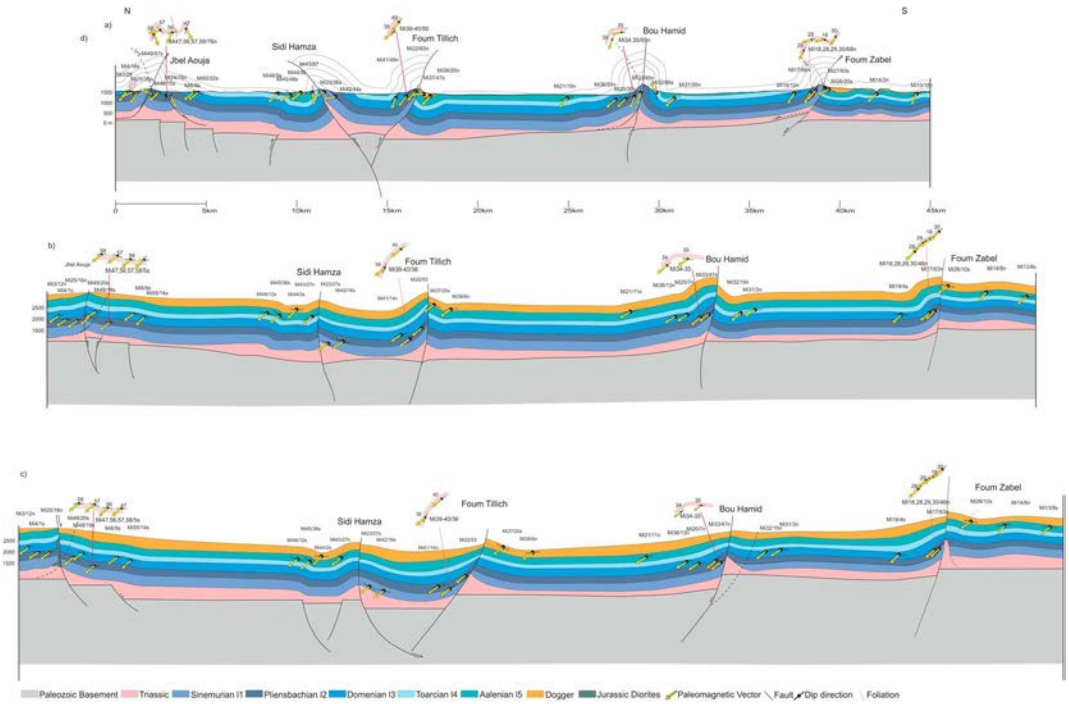

Figure 8. (a) Present-day cross section of the Midelt-Errachidia profile. The paleomagnetic sites, bedding (black lines), and paleomagnetic vectors (arrows) are indicated. (b) Transpressive end-member restored section at 100 Ma. (c) Extensional/diapiric end-member restored section at 100 Ma.

Once the paleodips at the time of remagnetization were obtained (Table 1), they were projected onto the vertical plane of the cross section considering the stratigraphic positions of the samples within the sedimentary pile, obtaining a picture (Figure 8) of each transect at the remagnetization time (100 Ma).

7. Tectonic Reconstruction of the Midelt-Errachidia Cross Section

7.1. Present-Day Geometry

The first step for reconstructing the pre-100 Ma deformational stage is the accurate definition of the present-day geometry of the Midelt-Errachidia cross section. The existing reconstructions (Benammi, 2002; Teixell et al., 2003, see Figure 1) propose either involvement of the basement in all the structures, with significant highs and lows of its top (Teixell et al., 2003), or, alternatively, fault-related folds linked to a subhorizontal, interestratal detachment, but also rooted in the basement (Benammi, 2002). In our opinion, there are several facts that must be taken into account and that any feasible model for the present-day state must respect:

a The cores of the synclines are occupied by Upper Lias or Dogger materials, and rocks of equivalent age are located at similar elevations in these cores (Figure 1b). This means that the top of the basement cannot be at very different elevations or, even less, reproduce the geometry of the folds at surface. We will come back to this latter issue. An argument in favor of the involvement of the basement (Teixell et al., 2003) is the Paleozoic core of the Mougueur culmination, located some kilometers east of the presented cross section. However, the westward plunge of this structure, together with the quick changes of the geometry of structures along trend, precludes the extrapolation of this uplift to the presented cross section.

b The anticlines are tight (Figure 8), most of them show steeply dipping faults and thrusts in their cores, and in some cases (Bou Hamid structure) practically isoclinal. Vergence of high-angle thrusts located in their cores commonly changes along trend. These features are consistent with the presence of a ductile level in the core of anticlines, thus implying a strong decoupling from the top of the basement.

c Angular relationships between the two walls in thrusts cutting the cores of the anticlines (Table 2) are not consistent with fault-related folds (fault-propagation or fault-bend folds, see, e.g., Jamison, 1992). Instead, a consistent kinematic model must consider either an initial stage of detachment folding (by

Table 2
Specific Structural Characteristic of the Section Midelt-Errachidia

Structure (from N to S)	Hanging wall bedding dip/geometry	Footwall bedding dip	Probable thrust dip	Vergence (along the cross section)
Jbel Aouja	35 N low-angle ramp	87 S flat (?)	35 N to 70 N	South
Sidi Hamza	36 S ramp	87 N ramp	70 S-90	North
Foum Tillich	83 N ramp	47 S ramp	70 S	South
Bou Hamid	85 N low-angle ramp	86 S low-angle ramp	90 (diminishing at depth)	South
Foum Zabel	66 S flat	63 S ramp	66 S	South

compressional or diapiric mechanisms) or an out-of-plane movement of material (because of strike slip or transpression) that accounts for the incompatibility between folds and associated thrusts.

According to these constraints, our reconstruction of the present-day structure of the Midelt-Errachidia cross section (Figure 8) shows a regular, though not completely flat basement top, and we consider that most of the thrusts involving the Mesozoic cover branch at depth in the Upper Triassic detachment. We do not discard, however, a moderate conditioning by some basement structures that could be responsible for structuring the Jurassic basin during the extensional stage. The proposed geometry is therefore an intermediate between the two formerly proposed end members: (i) a rigid basement cut by noninverted normal faults clearly decoupled from the tightly folded sedimentary cover (Benammi, 2002) and (ii) heterogeneous basement-involved structures with limited role of the detachment (Teixell et al., 2003) and inverted normal faults (Missenard, 2006). Some of these inherited faults could have acted as stress raisers, facilitating the development of structures in the overlying cover. The proposed geometry implies the local thickening of the detachment level under some structures, what can aid to interpret some gravity lows of the residual gravity anomaly along the transect (see, e. g. Ayarza et al., 2005 for the Bouguer gravimetric profile). Anyway, it must be taken into account that the combination of high (basalts and gabbros) and low (salts) density bodies, as well as the high density of the Jurassic limestones, often preclude the direct application of gravity methods in these areas.

An unknown variable is the change in thickness of Jurassic sedimentary units from the anticline crests to the core of the synclines, and, because of the scarcity of subsurface data, it is difficult to constrain. As mentioned in the stratigraphic description of materials, there are some hints that support the existence of an undetermined thickening of some units, and that it is probable for the detachment level to be thinner at the core of the synclines.

7.2. Reconstruction at 100 Ma

The calculation of paleodips along the Midelt-Errachidia cross-section (Figure 8a) allows us to obtain a configuration of the structures at the age of 100 Ma. However, for particular paleodips at the limbs of structures, different possible reconstruction of the structures can be obtained, depending on the processes involved in their formation. In our sections, two different possible scenarios were considered since both are compatible with our results: (i) transpression during the Late Jurassic and Early Cretaceous (Figure 8b) and (ii) early diapirism related to extensional tectonics (Figure 8c). The main differences between cross sections considering the two different mechanisms are the volume of evaporites at the core of anticlines/diapirs in the restored configuration, even considering similar dips of beds, and the thickening of units toward the basin center during the remagnetization stage, that would be probably higher for the extension/diapirism hypothesis. The cross section was divided into four detailed restored profiles to show specific features of the five studied ridges. Structures will be described from north to south.

In the Jbel Aouja present-day profile (Figure 9a) a south-verging harpoon structure whose southern flank overthrusts finally its northern flank, with a fault-propagation fold geometry, can be interpreted. A second, north-verging harpoon structure is associated with fault reactivation (Figure 9a). The hinge of the ridge is cut by a high angle fault, with the lowermost part of the Lower Lias (l1) cropping out in its northern flank and the middle part of the Lower Lias (l2) in its southern flank. It also shows two metric-scale folds clearly related to the Cenozoic compression.

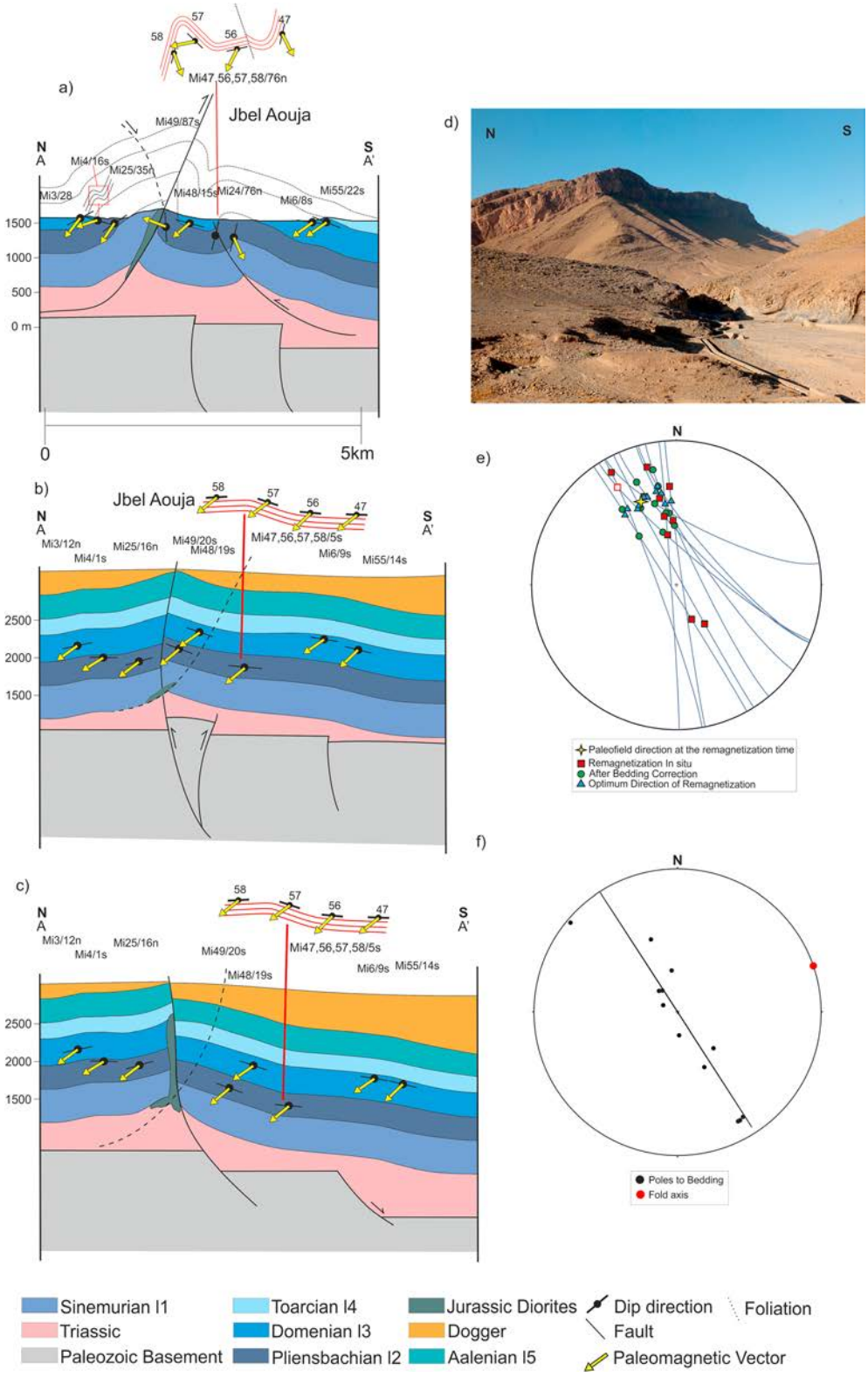

Figure 9. (a) Present-day cross section of the Jbel Aouja Ridge. The paleomagnetic sites, bedding, and paleomagnetic vectors are indicated. (b) Transpressive end-member restored section at 100 Ma. (c) Extensional/diapiric end-member restored section at 100 Ma. (d) Field photography of the structure of the Jbel Aouja (south-verging thrust associated with the northernmost anticline). (e) Stereoplot showing the small circle corresponding to the restored remagnetization directions from selected sites. The symbols are the same as those shown in Figure 6. (f) Stereoplot showing poles of bedding of the structure.

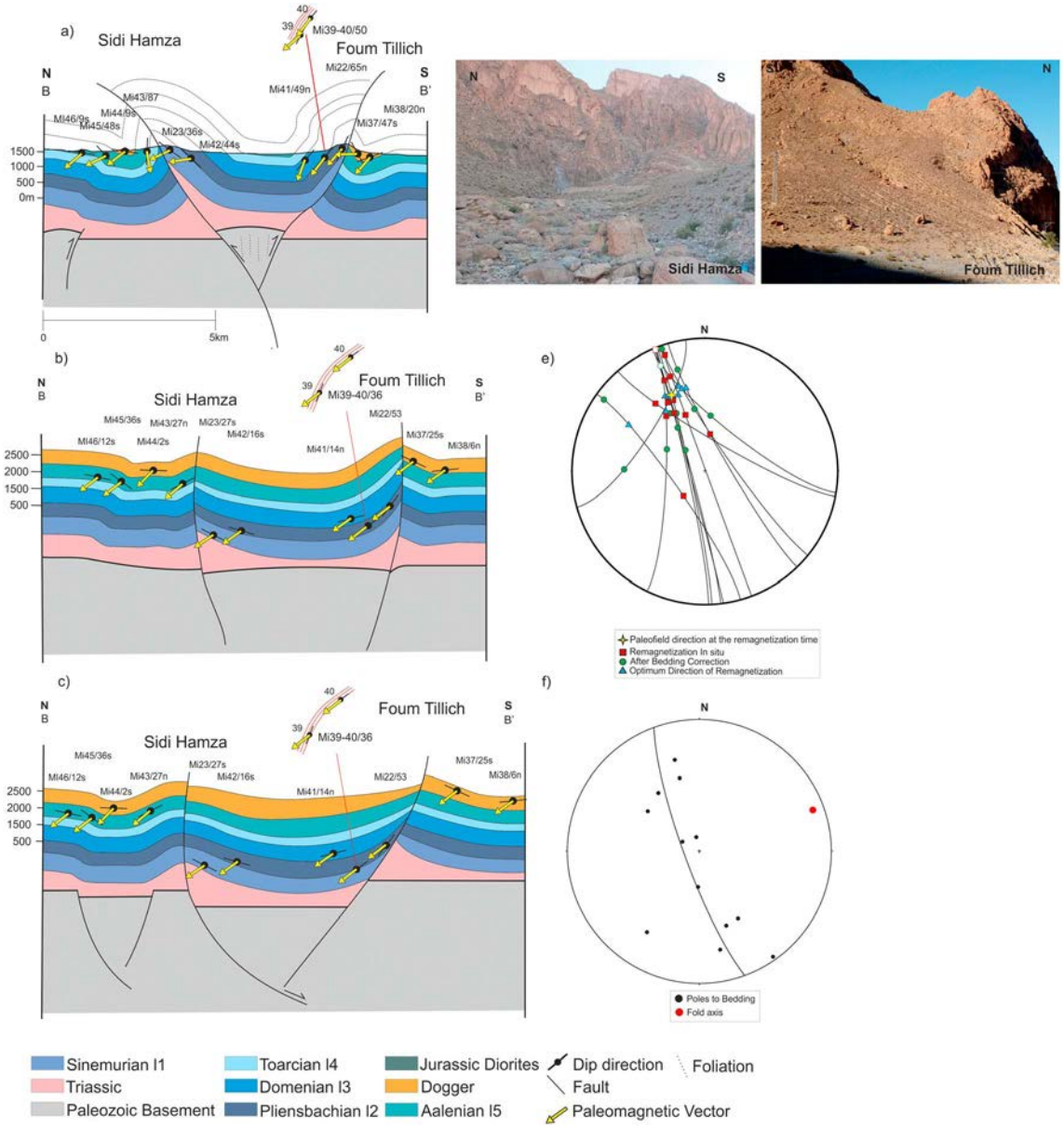

Figure 10. (a) Present-day cross section of the Sidi Hamza and Foum Tillich ridges. The paleomagnetic sites, bedding, and paleomagnetic vectors are indicated. (b) Transpressive end-member restored section at 100 Ma. (c) Extensional/diapiric end-member restored section at 100 Ma. (d) Field photography of the structures at Sidi Hamza (southern, back-limb of the thrusted anticline) and Foum Tillich (hectometer-scale back thrust in its northern limb). (e) Stereoplot showing the small circle corresponding to the restored remagnetization directions from selected sites. The symbols are the same as those shown in Figure 6. (f) Stereoplot showing poles of bedding of the structure.

The 100-Ma geometry of this structure (Figures 9b and 9c) in the transpressional and extensional reconstructions are very similar, showing a gentle profile with incipient reverse or normal faulting. The small-scale fold (sites 47, 56, 57, and 58) developed completely during the Cenozoic inversion, since in the palinspastic reconstruction beds are flat and shallowly dipping to the South.

The Sidi Hamza and Foum Tillich anticlines (Figure 10a) define altogether a pop-up structure. The Sidi Hamza anticline shows a northward vergence, and its hinge is cut by a high-angle fault. In its southern flank, the Lower Lias (l1) overlies the Upper Lias (l3) reaching dips up to 87°. The Foum Tillich structure shows a southward vergence and is also affected by a high angle reverse fault. The lower Lias (l1) is nearly vertical while the dip of the Dogger units in the footwall does not exceed 45°. The northern flank of Sidi Hamza and the southern flank of Foum Tillich define an asymmetric syncline.

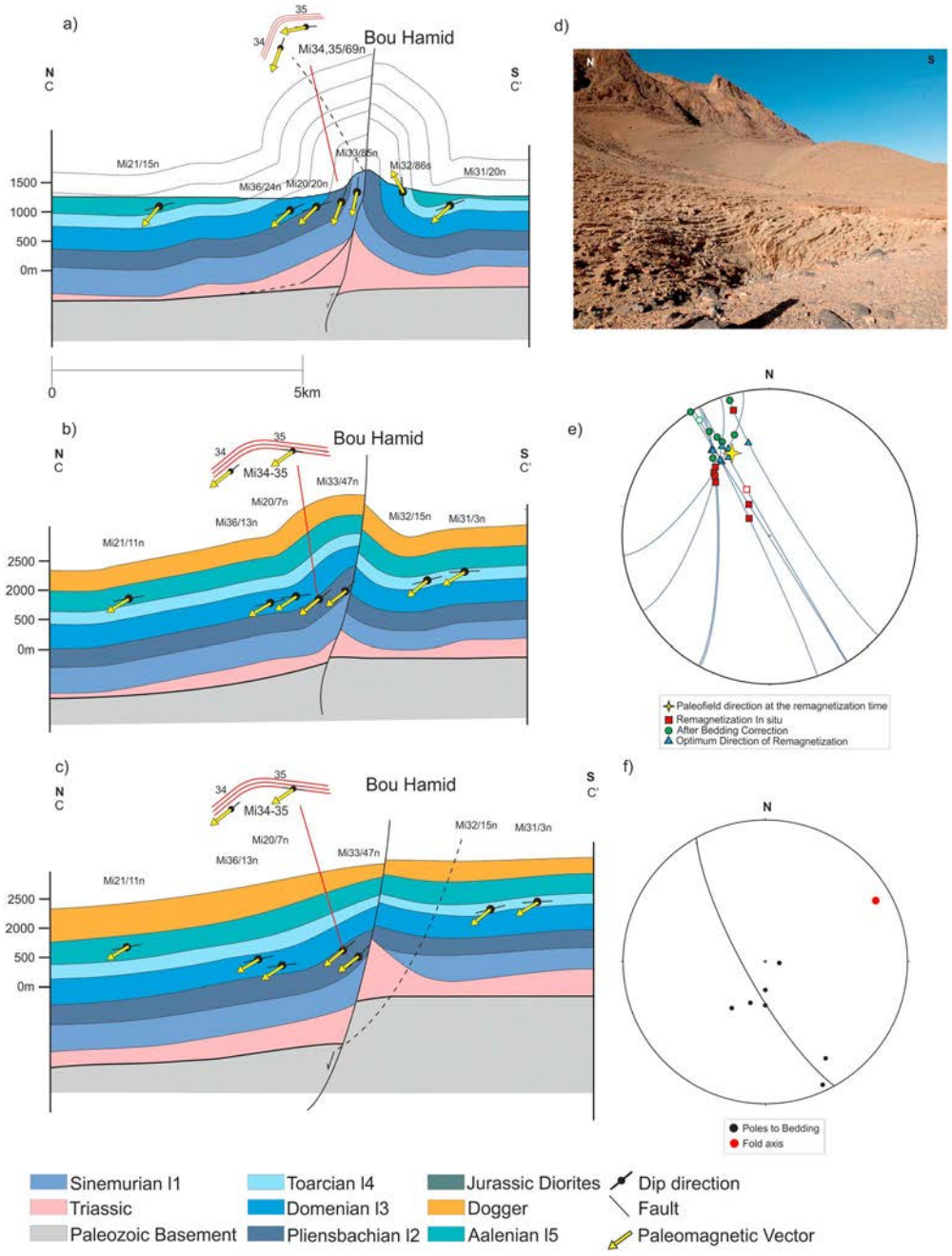

Figure 11. (a) Present-day cross section of the Bou Hamid ridge. The paleomagnetic sites, bedding, and paleomagnetic vectors are indicated. (b) Transpressive end-member restored section at 100 Ma. (c) Extensional/diapiric end-member restored section at 100 Ma. (d) Field photography of the southern limb of the Bou Hamid anticline. (e) Stereoplot showing the small circle corresponding to the restored remagnetization directions from selected sites. The symbols are the same as those shown in Figure 6. (f) Stereoplot showing poles of bedding of the structure.

The restored cross sections (Figures 10b and 10c) indicate that the described structure was already developed before the Cenozoic inversion. A syncline with box-fold geometry is interpreted in the northern flank of the Sidi Hamza Ridge. A harpoon structure is observed in the Foum Tillich Ridge showing dips up to 53°. The different structures can be explained either by transpression (Figure 10b) or diapirs showing salt-wall geometry (Figure 10c). The reconstruction of the small-scale fold shows that it developed at 100 Ma.

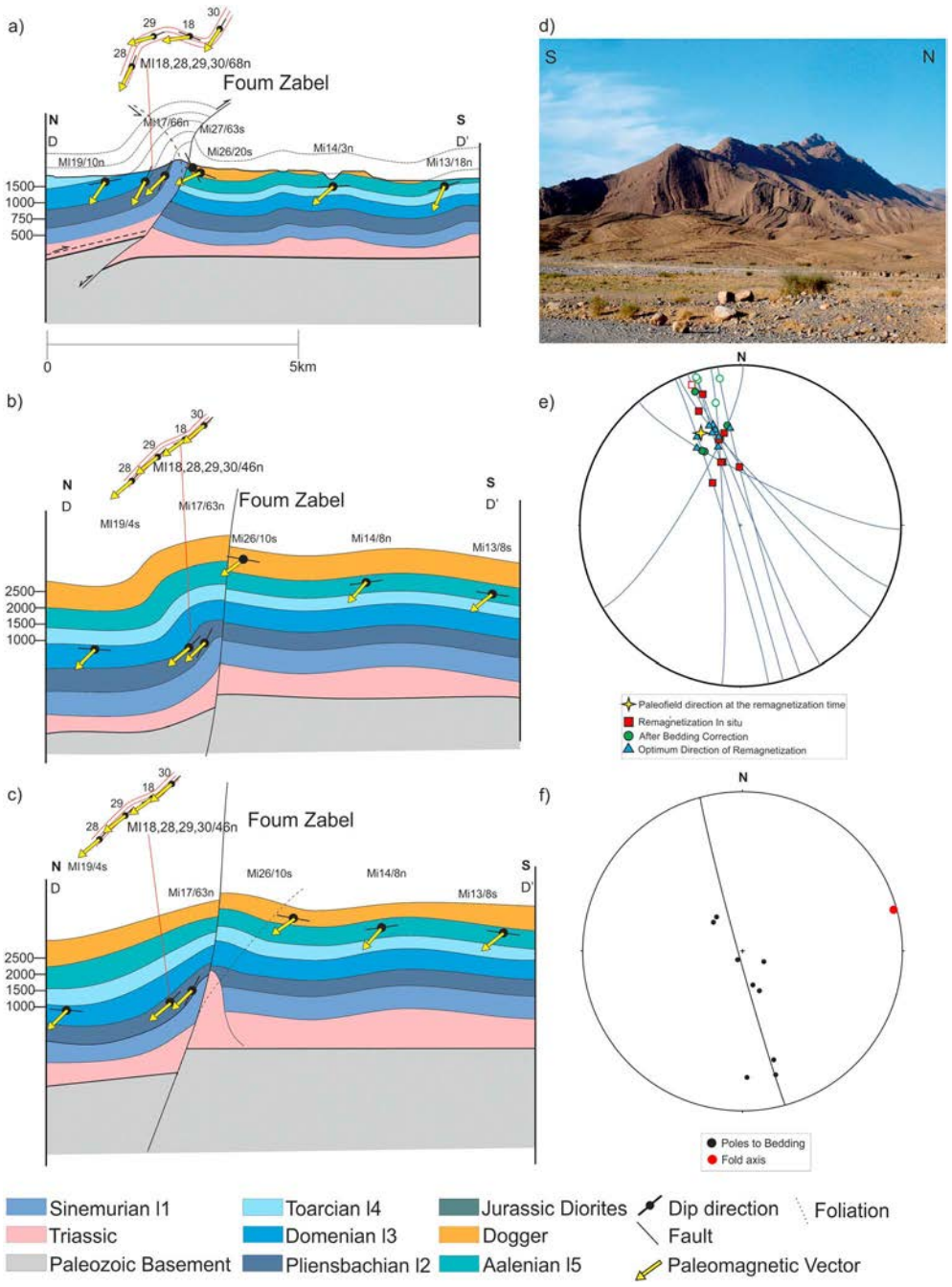

Figure 12. (a) Present-day cross section of the Foum Zabel ridge. The paleomagnetic sites, bedding, and paleomagnetic vectors are indicated. (b) Transpressive end-member restored section at 100 Ma. (c) Extensional/diapiric end-member restored section at 100 Ma. (d) Field photography of the northern (back) limb of the faulted anticline at Foum Zabel. (e) Stereoplot showing the small circle corresponding to the restored remagnetization directions from selected sites. The symbols are the same as those shown in Figure 6. (f) Stereoplot showing poles of bedding of the structure.

The Bou Hamid anticline is an upright, nearly symmetric box-fold in the present-day cross section (Figure 11a), having dips up to 86° and cut by a high angle fault. In the 100-Ma reconstruction, this anticline can be interpreted as a fault-propagation fold (Figure 11b) with an already developed harpoon structure, or alternatively as a symmetric diapir (Figure 11c) probably associated with extension. The metric-scale fold in its northern flank tightened after remagnetization time.

The Foum Zabel is a fault-propagation fold, and its present-day geometry is similar to the other anticlines. It can be classified as a high angle break-through fold. Its core is occupied by Triassic rocks (Figure 12a). It shows a southward vergence, with a northern flank dipping up to 68° and formed by Lower Lias, and a southern flank formed by Dogger limestones reaching dips of 63°.

In the 100-Ma reconstruction (Figures 12b and 12c), its southern flank presents moderate dips and the Dogger beds are more or less subhorizontal, while its northern limb shows dips up to 46°. A reverse fault or alternatively a salt-wall can explain the Foum Zabel configuration at this stage. The smaller scale fold developed completely during the compressional Cenozoic stage, but an inherited significant southward dip can be inferred from the restored sketch.

Paleomagnetic data thus indicate that the five studied ridges in the Midelt-Errachidia profile were partially developed at 100 Ma, although each underwent a different evolution. Curiously, the central ridges, Foum Tillich and Bou Hamid, were more developed at 100 Ma, including some of the smaller-scale folds at the limbs of the main structures.

8. Discussion

8.1. Origin of the Remagnetization

The mechanisms that trigger sedimentary remagnetizations have generated numerous studies in recent years but nowadays are still an open question. Torres-López et al. (2014) established that the widespread remagnetization of the limestones from the Central high Atlas is of chemical origin related to growing of diagenetic magnetite. Widespread remagnetizations in carbonates are documented in different regions being the more renowned example the one observed in Paleozoic carbonate strata from the Appalachian Basin (McCabe & Elmore, 1989a). These remagnetizations are also carried by neo-formed magnetite showing a very particular magnetic signature (McCabe & Channell, 1994a; Dunlop, 2002) similar to the one described above (Figure 3d). This type of remagnetizations has been associated with burial processes (Aubourg et al., 2008, 2012; Evans et al., 2000; Katz et al., 1998; Woods et al., 2000, 2002) and also to pressure solutions structures within the burial context (Evans et al., 2000). Torres-López et al. (2014) pointed out that the remagnetization process in the Central High Atlas involves (1) basin-scale conditions mainly related to a minimum thickness of sediments and (2) a regional-scale thermal event acting as a catalyst of remagnetization. In any case, the mechanism must be associated with cooling below a critical temperature because there are no differences in magnetic properties or paleomagnetic directions despite the differences in the position within the stratigraphic sequence of the different sites within the basin. If remagnetization occurs independently of age (position) and type of sediment, small variations in thickness, and therefore in pressure and temperature, must be conditioning factors to block this process. The cooling necessary to block the magnetization could be achieved either by partial inversion of the basin (transpressional hypothesis; see below) or by decreasing of the temperature gradient and thermal re-equilibration of the continental crust (extensional-diapirism hypothesis; see below).

8.2. Geodynamic Processes at Debate

The principal tectonic stages underwent by the Central High Atlas are documented by numerous authors, but there is a controversial point in the tectonic activity during the Mesozoic. This debate is open since Jacobshagen et al. (1988) exposed that inversion processes started at the end of the Oligocene (Laville & Piqué, 1992), thus contradicting Studer and Du Dresnay (1980) that pointed out intra-Jurassic compressional movements. Mesozoic, syn-sedimentary movements were first described by Dubar (1938) and related to Late Liassic and Middle Jurassic horizontal compression by Studer and Du dresnay (1980).

Laville and Piqué (1992) defended the existence of Jurassic deformation based on the development of cleavage near intrusive bodies before the deposition of Late Jurassic red beds and pointed out that emplacement of gabbro bodies contemporaneous with Jurassic deformation was a related process. Ibouh et al. (1994, 2001) recognized in the Imilchil area (60 km west of the studied cross section) a compressional phase during the Bajocian. A mechanism for this particular tectonic stage was proposed by Laville et al. (2004), who indicated that the transpressive regime in the High Atlas during the Middle Jurassic was associated to the sinistral movement of Africa relative to Eurasia. Other authors (Beauchamp et al., 1996; Beauchamp et al., 1999; Bertotti & Gouiza, 2012) also admit uplifting of the Central High Atlas during this time, which would cause syn-sedimentary deformations (also described, e.g., by Ettaki et al., 2007 and Gouiza et al., 2010). Finally, thermal modeling and interpretation of igneous intrusions (Gouiza et al., 2010; Charton et al., 2018) point to a

relationship between transpression and magmatism, on one side, and to the exhumation of the onshore domain in the margin Atlantic of Morocco from Permian to Jurassic times, on the other.

Calvín, Casas-Sainz, et al. (2017) using the method of Villalaín et al. (2016) relate cleavage, folding, and Cretaceous deformation and show the geometry at 100 Ma in different areas of the Central High Atlas. In all cases, cleavage postdates the remagnetization and can therefore be interpreted as generated during the Cenozoic inversion. However, the reconstruction of folds shown by these authors indicates preremagnetization incipient folds, which can be due to an intra-Mesozoic compressional event. However, this compressional, intermediate stage is still controversial and not recognized by other authors (see e.g., Gómez et al., 2002, Ellouz et al., 2003, Teixell et al., 2003, Arboleya et al., 2004, Barbero et al., 2007, Frizon de lamotte et al., 2008, Michard et al., 2008., Babault et al., 2013, Bensalah et al., 2013), who defend that in The Central High Atlas there has only been one inversion stage in Cenozoic times.

The scarcity or absence of Upper Jurassic and Cretaceous sedimentary record in the Central High Atlas makes difficult the field observations to determine the possible intra-Jurassic deformations.

8.3. Cross-Section Reconstruction

The High Atlas underwent a remagnetization during the quiescent period bracketed between the end of rifting (Middle Jurassic) and the compressional stage (Cenozoic) related to collision tectonics. Therefore, the events occurring between syn-rift deformation (here including folding associated with normal faults, diapirs, and igneous intrusions; Teixell et al., 2003; Michard et al., 2008) and wholesale compressional folding and thrusting during the Cenozoic can be considered as "syn-tectonic" (from the paleomagnetic point of view) and can reveal Mesozoic deformations not known at present. Moreover, the evolution during the Late Jurassic and Early Cretaceous is poorly constrained due to the disperse nature of the sedimentary record that generally appears within isolated outliers and marginal areas of the High Atlas.

The Midelt-Errachidia profile shows typical features of the Central High Atlas: fault-thrust systems with NE-SW to E-W trends showing sinuous, anastomosing traces, and varying polarity (i.e., north-verging and south-verging steeply dipping thrusts at the core of anticlines). These characteristics are commonly found in inverted basins resulting from extensional oblique tectonic contexts, as the one that occurred during Triassic and Early Jurassic times in the Moroccan Atlas. The anticlines (ridges) are narrow and cut by high-angle faults, resulting from the reactivation of previous extensional faults. Between them, there are broad, gentle synclines. In general, the northern flanks of the ridges present steeper dips and are defined by Lower Lias limestones, while their southern flanks show shallower dips and are defined by Upper Lias and Dogger limestones.

Palinspastic reconstructions of cross sections indicate that the geometry of ridges at 100 Ma was already initiated. It is observable that the steep paleodips are distributed toward the central and southern sectors of the basin, whereas in the north, these paleodips are much gentler. It is to notice that the Dogger units (Bajocian and Bathonian limestones) are also folded and do not fossilize previous structures. We also observe that high angle, break-through faults associated with folds were partially developed at the remagnetization time. In restored cross sections, dips up to 50° have been obtained. These steep dips are difficult to explain within an extensional tectonic context lacking gabbroic intrusion or salt walls or diapirs characteristic of other regions of the High Atlas.

Torres-López et al. (2016) reconstructed quantitatively the amount of folding in three structures of the Central High Atlas in the Imilchil area: the Tassent, Tasraft, and Tissila ridges at the age of the Cretaceous remagnetization. These authors pointed out different evolutionary trends for each structure and concluded that folding during the Mesozoic basinal stage was heterogeneously distributed along the chain and related to gabbro intrusions and diapirs nucleating the core of the anticlines.

The present work shows that along the Midelt-Errachidia cross section, structures were incipiently developed at 100 Ma. The main difference with the Imilchil area is the absence of gabbroic bodies and diapiric walls in the present-day situation. Although the whole Central High Atlas is an extensive diapiric province (Saura et al., 2014), the Upper Triassic evaporitic level thins toward the E-ESE (Saura et al., 2014), and the presence of the gabbroic bodies is also limited to the central area of the Central High Atlas (Guezal et al., 2011; Bensalah et al., 2013; Frizon de Lamotte et al., 2008).

The restored cross sections indicate that the paleodips obtained are consistent with two different models of Mesozoic tectonism: transpression and normal faulting associated with diapirism. Transpressional regime was associated with thick skinned deformation involving the basement and a general detachment level in the Triassic series; most part of the faults in the sedimentary cover are reactivated and inverted (Figure 8). This reactivation involved the formation of harpoon, pop up structures, and box folds. In the end-member diapiric interpretation, the basement is affected by extensional faults, and salt walls associated with normal faults or simple diapirs are responsible for the paleodips obtained at 100 Ma. According to the feasibility of the different reconstructions (Figure 8) the most probable scenario is a combination of both origins, with some structures (Foum Zabel and Jbel Aouja, and probably Bou Hamid) growing at the basin margins associated with normal faults, salt walls, and probably thickness changes within the sedimentary pile, whereas other ridges (namely Sidi Hamza and Foum Tillich) fit better with a transpressional origin that is also consistent with cartographic patterns in geological maps (Ahmed et al., 1956).

9. Conclusions

This study provides 43 new sites with paleomagnetic data corroborating that the remagnetization found in other parts of the chain extends at least to the easternmost part of the Central High Atlas, showing systematically normal polarity. Fold tests indicate that remagnetization is syn-folding in relation to some structures and clearly predates the Cenozoic compressional stage. The characteristic direction of the remagnetization is calculated by the SCI method, (Dec: 337.3, Inc: 38.4, η: 13.0, ξ: 3.5, A/n: 7.7°) through pySCu software (Calvín, Villalaín, et al., 2017). Comparison with the direction from the African GAPWP obtained by Torsvik et al. (2012) provides an age for the remagnetization at 100 Ma.

This syn-folding remagnetization allows obtaining the geometry of the basin at 100 Ma using the method developed by Villalaín et al. (2016). We provide a palinspastic picture of one of the best studied profiles in the Central High Atlas, through four detailed cross section of ridges considering two different scenarios. The results obtained on the five ridges show that they were initiated prior to compressive deformation during the Late Cretaceous-Cenozoic and that compressional folds nucleated on these incipient structures.

This work highlights the deformations occurred during the Late Jurassic in the easternmost part of the Central High Atlas. We cannot prove whether folding observable at 100 Ma is due to the accommodation to basement faults and salt-wall formation within a transtensional/extensional regime or, alternatively, due to uplifting of the Central High Atlas during Middle-Late Jurassic weak transpressive intra-Jurassic tectonics. However, in our opinion, the restored sections of the Jbel Aouja, Sidi Hamza-Foum Tillich, Bou Hamid, and Foum Zabel ridges show that structures located at the basin margins fit better with extension and diapirism, whereas the ridges in the central sector (Sidi Hamza-Foum Tillich) are consistent with transpression at the basin center. This situation could be related to the blocking of the remagnetization at 100 Ma.

Acknowledgments
This study was financed by the research projects CGL2012-38481 and CGL2016-77560 of the MINECO (Spanish Ministry of Economy and Competitiveness) with also FEDER founding (European Union). Sara Torres-López acknowledges the financial support given by the grant of FPI by the Ministerio de Economía y Competitividad of the Spanish government. The data used are listed in the table.

References

Ahmed, M. M., Eyssautier, L., Marçais, J., Choubert, G., & Fallot, P. (1956). Carte Géologique du Haut Atlas: feuilles Rich et Boudenib. Service Géologique du Maroc.

Ait Addi, A., & Chafiki, D. (2013). Sedimentary evolution and palaeogeography of mid-Jurassic deposits of the Central High Atlas, Morocco. *Journal of African Earth Sciences*, *84*, 54–69.

Arboleya, M. L., Teixell, A., Charroud, M., & Julivert, M. (2004). A structural transect through the High and Middle Atlas of Morocco: Tectonic implications. *Journal of African Earth Science*, *39*(3-5), 319–327. https://doi.org/10.1016/j.jafrearsci.2004.07.036

Aubourg, C., Pozzi, J.-P., Janots, D., & Sarahoui, L. (2008). Imprinting chemical remanent magnetization in claystones at 95 8C. *Earth and Planetary Science Letters*, *272*(1-2), 172–180. https://doi.org/10.1016/j.epsl.2008.04.038

Aubourg, C., Pozzi, J.-P., & Kars, M. (2012). Burial, claystones remagnetizations and some consequences for magnetostratigraphy. In: Elmore, R.D., Muxworthy, A.R., Aldana, M.M. & Mena, M. (eds) remagnetization and chemical alteration of sedimentary rocks. *Geological Society, London, Special Publications*, *371*(1), 181–188. https://doi.org/10.1144/SP371.4

Ayarza, P., Alvarez-Lobato, F., Teixell, A., Arboleya, M. L., Teson, E., Julivert, M., & Charroud, M. (2005). Crustal structure under the central High Atlas Mountains (Morocco) from geological and gravity data. *Tectonophysics*, *400*(1–4), 67–84.

Babault, J., Teixell, A., Struth, L., Van Den Driessche, J., Arboleya, M. L., & Tesón, E. (2013). Shortening, structural relief and drainage evolution in inverted rifts: Insights from the Atlas Mountains, the Eastern Cordillera of Colombia and the Pyrenees. *Geological Society, London, Special Publications*, *377*, 14.

Barbero, L., Teixell, A., Arboleya, M.-L., Del Rio, P., Reiners, P. W., & Bougadir, B. (2007). Jurassic-to-present thermal history of the Central High Atlas (Morocco) assessed by low-temperature thermochronology. *Terra Nova*, *19*(1), 58–64. https://doi.org/10.1111/j.1365-3121.2006.00715.x

Beauchamp, W., Allmendinger, R., Barazangi, M., Demnati, A., El Alji, M., & Dahmani, M. (1999). Inversion tectonics and the evolution of the High Atlas Mountains, Morocco, based on a geological-geophysical transect. *Tectonics*, *18*(2), 163–184. https://doi.org/10.1029/1998TC900015

Beauchamp, W., Barazangi, M., Demnati, A., & El Alji, M. (1996). Intracontinental rifting and inversion: Missour Basin and Atlas Mountains, Morocco. *American Association of Petroleum Geologists Bulletin*, *80*, 1459–1482.
Benammi, M. (2002). La chaîne Atlasique Marocaine. Evolution géodynamique meso-cenozoïque du haut Atlas central et de sa zone de junction avec le Moyen Atlas Meridional (Maroc). PhD Thesis, University Ibn Tofail.
Bensalah, M. K., Youbi, N., Mata, J., Madeira, J., Martins, L., El Hachimi, H., et al. (2013). The Jurassic-Cretaceous basaltic magmatism of the Oued El-Abid syncline (High Atlas, Morocco): Physical volcanology, geochemistry and geodynamic implications. *Journal of African Earth Science*, *81*, 60–81. https://doi.org/10.1016/j.jafrearsci.2013.01.004
Bertotti, G., & Gouiza, M. (2012). Post-rift vertical movements and horizontal deformations in the eastern margin of the Central Atlantic: Middle Jurassic to Early Cretaceous evolution of Morocco. *International Journal of Earth Sciences*. (Geol Rundsch) (2012), *101*, 2151–2165. https://doi.org/10.1007/s00531-012-0773-4
Bracène, R., & Frizon de Lamotte, D. (2002). The origin of intraplate deformation in the Atlas system of western and central Algeria: From Jurassic rifting to Cenozoic-Quaternary inversion. *Tectonophysics*, *357*(1-4), 207–226. https://doi.org/10.1016/S0040-1951(02)00369-4
Calvín, P., Casas-Sainz, A. M., Villalaín, J. J., & Moussaid, B. (2017). Diachronous folding and cleavage in an intraplate setting (Central High Atlas, Morocco) determined through the study of remagnetizations. *Journal of Structural Geology*, 97.1e17.
Calvín, P., Villalaín, J. J., Casas-Sainz, A. M., Tauxe, L., & Torres-López, S. (2017). pySCu: A new python code for analyzing remagnetizations directions by means os Small Circle utilizes. *Computational Geosciences*, *109*. https://doi.org/10.1016/j.cageo.2017.07.002
Casas, A. M., Villalaín, J. J., Soto, R., Gil-Imaz, A., Del Río, P., & Fernández, G. (2009). Multidisciplinary approach to an extensional syncline model for the Mesozoic Cameros Basin (N Spain). *Tectonophysics*, *470*(1-2), 3–20. https://doi.org/10.1016/j.tecto.2008.04.020
Chadima, M., & Hrouda, F. (2006). Remasoft 3.0 a user-friendly paleomagnetic data browser and analyzer. Trav. *Geophysical*, *27*, 20e21.
Channell, J. E. T., & McCabe, C. (1994). Comparison of magnetic hysteresis parameters of unremagnetized and remagnetized limestones. *Journal of Geophysical Research*, *99*(B3), 4613–4623. https://doi.org/10.1029/93JB02578
Charton, R., Bertotti, G., Arantegui, A., & Bulot, L. (2018). The Sidi Ifni transect across the rifted margin of Morocco (Central Atlantic): Vertical movements constrained by low-temperature thermochronology. *Journal of African Earth Sciences*, *141*, 22–32.
Choubert, G., & Faure-Muret, A. (1962). Evolution du domaine atlasique marocain depuis les temps paleozoiques. In: Evolution du domaine atlasique marocain depuis les temps paléozoïques, livre à la mémoire du Prof. P. Fallot. *Memoire hors-serie, Service de la Societe Geologique de France*, *1*, 447–514.
Day, R., Fuller, M., & Schmidt, V. A. (1977). Hysteresis properties of titanomagnetites: grain-size and compositional dependence. *Physics of the Earth and Planetary Interiors*, *13*(4), 260–267.
Dubar, G. (1938). Sur la formation de rides à l'Aalénien et au Bajocien dans le Haut Atlas de Midelt. *Comptes Rendus de l'Académie des Sciences*, *206*, 525–527.
Dunlop, D. J. (2002). Theory and application of the day plot (Mrs/Ms v. Hcr/Hc). 2. Application to data for rocks, sediments, and soils. *Journal of Geophysical Research*, *107*(3B), 2057. https://doi.org/10.1029/2001JB000486
El Harfi, A., Guiraud, M., & Lang, J. (2006). Deep-rooted 'thick skinned' model for the High Atlas Mountains (Morocco). Implications for the structural inheritance of the southern Tethys passive margin. *Journal of Structural Geology*, *28*, 1958–1976.
El Harfi, A., Lang, J., Salomon, J., & Chellai, E. H. (2001). Cenozoic sedimentary dynamics of the Ouarzazate foreland basin (Central High Atlas Mountains, Morocco). *International Journal of Earth Sciences*, *90*, 393e411.
Ellouz, N., Patriata, M., Gauliera, J. M., Bouatmanib, R., & Sabounji, S. (2003). From rifting to Alpine inversion: Mesozoic and Cenozoic subsidence history of some Moroccan basins. *Sedimentary Geology*, *156*(1-4), 185–212. https://doi.org/10.1016/S0037-0738(02)00288-9
Ettaki, M., Ibouh, H., Chellaï, E. H., & Milhi, A. (2007). Liassic diapiric structures from the Central High Atlas, Morocco; Ikerzi ride example. *Africa Geoscience Review*, *14*, 79–93.
Evans, M. A., Elmore, R. D., & Lewchuk, M. T. (2000). Examining the relation-ship between remagnetization and orogenic fluids: Central Appalachians. *Journal of Geochemical Exploration*, *69-70*, 139–142. https://doi.org/10.1016/S0375-6742(00)00120-5
Fisher, R. A. (1953). Dispersion on a sphere. *Proceedings of the Royal Society of London*, *217A*, 295–305.
Frizon de Lamotte, D., Leturmy, P., et al. (2008). Mesozoic and Cenozoic vertical movements in the Atlas system (Algeria, Morocco, Tunisia): An overview. *Tectonophysics*, *475*, 9–28.
Frizon de Lamotte, D., Saint Bézar, B., Bracéne, R., & Mercier, E. (2000). The two main steps of the Atlas building and geodynamics of the western Mediterranean. *Tectonics*, *19*(4), 740–761. https://doi.org/10.1029/2000TC900003
Gómez, F., Beauchamp, W., & Barazangi, M. (2002). Role of the Atlas Mountains (northwest Africa) within the African-Eurasian plate-boundary zone. *Geology* 2000, *28*(9), 775–778. https://doi.org/10.1130/0091-7613
Gouiza, M., Bertotti, G., Hafid, M., & Cloetingh, S. (2010). Kinematic and termal evolution of the Moroccan rifted continental margin: Doukkala-High Atlats transect. *Tectonics*, *29*, TC5008. https://doi.org/10.1029/2009TC002464
Guezal, J., El Baghdadi, M., Barakat, A., & Raïs, J. (2011). Le magmatisme jurassique- crétacé de Béni-Mellal (Haut- Atlas Central, Maroc): géochimie et signification géodynamique. Bulletin de l'Institut Scientifique, section. *Sciences de la Terre*, *33*, 17–23.
Ibouh, H., Bouabdelli, M., & Zargouni, F. (1994). Indices de tectonique synsédimentaire dans les dépôts aaléno-bajocien de la région d'Imilchil (Haut Atlas Central, Maroc). *Miscellanea Servo Geologia Nazionale Roma*, *5*, 305–310.
Ibouh, H., El Bchari, F., Bouabdelli, M., Souhel, A., & Youbi, N. (2001). L'accident tizal-azourki haut atlas central du maroc: déformations synsédimentaires liasiques en extension et conséquences du serrage atlasique. *Estudios Geologicos*, *57*(1–2), 15–30.
Jackson, M. (1990). Diagenetic sources of stable remanence in remagnetized Paleozoic cratonic carbonates: A rock magnetic study. *Journal of Geophysical Research*, *95*(B3), 2753–2761.
Jacobshagen, V., Görler, K., & Giese, P. (1988). Geodynamic evolution of the Atlas System (Morocco) in post-Palaeozoic times. In *The Atlas System of Morocco* (pp. 481–499). Berlin, Heidelberg: Springer.
Jamison, W. R. (1992). Stress controls on fold thrust style. In K. R. McClay (Ed.), *Thrust tectonics*, edited by, (pp. 155–164). New York: Chapman and Hall.
Katz, B., Elmore, R. D., Cogoini, M., & Ferry, S. (1998). Widespread chemical remagnetization: Orogenic fluids or burial diagenesis of clays? *Geology*, *26*(7), 603–606. https://doi.org/10.1130/0091-7613(1998)026<0603:WCROFO>2.3.CO;2
Kent, D. V. (1982). Paleomagnetic evidence for post-Devonian displacement of the Avalon Platform (Newfoundland). *Journal of Geophysical Research*, *87*(B10), 8709–8716.
Kent, D. V., & Opdyke, N. D. (1985). Multicomponent magnetizations from the Mississippian Mauch Chunk Formation of the Central Appalachians and their tectonic implications. *Journal of Geophysical Research*, *90*(B7), 5371–5383. https://doi.org/10.1029/JB090iB07p05371
Laville, E. (2002). Role of Atlas Mountains (northwest Africa) within the African-Eurasian plate-boundary zone: Comment. *Geology*, *30*(1), 95. https://doi.org/10.1130/0091-7613(2002)030<0095:ROTAMN>2.0.CO;2

Laville, E., Lesage, J. L., & Séguret, M. (1977). Geometrie, cinematique (dynamique) de la tectonique atlasique sur le versant sud du Haut Atlas marocain. Apercu sur les tectoniques hercyniennes et tardi-hercyniennes. *Bulletin de la Société Géologique de France*, *7*, 499–523.

Laville, E., & Piqué, A. (1992). Jurassic penetrative deformation and Cenozoic uplift in the Central High Atlas (Morocco): A tectonic model. Structural and orogenic inversions. *Geologische Rundschau*, *81*(1), 157–170. https://doi.org/10.1007/BF01764546

Laville, E., Piqué, A., Amrhar, M., & Charroud, M. (2004). A restatement of the Mesozoic Atlasic Rifting (Morocco). *Journal of African Earth Sciences*, *38*, 145–153.

Lowrie, W. (1990). Identification of ferromagnetic minerals in a rock by coercivity and unblocking temperature properties. *Geophysical Research Letters*, *17*(2), 159–162. https://doi.org/10.1029/GL017i002p00159

Mattauer, M., Proust, F., & Tapponier, P. (1972). Major strike-slip fault of late Hercynian age in Morocco. *Nature*, *237*(5351), 160–162. https://doi.org/10.1038/237160b0

Mattauer, M., Tapponier, P., & Proust, F. (1977). Sur les mecanismes de formation des chaines intracontinentales. L'exemple des chaines atlasiques du Maroc. *Bulletin de la Société Géologique de France*, *19*, 521–526.

McCabe, C., & Channell, J. E. T. (1994a). Late Paleozoic remagnetization in limestones of the Craven basin (northern England) and the rock magnetic fingerprint of remagnetized sedimentary carbonates. *Journal of Geophysical Research, B: Solid Earth*, *99*(B3), 4603–4612. https://doi.org/10.1029/93JB02802

McCabe, C., & Elmore, R. D. (1989a). The occurrence and origin of Late Paleozoic remagnetization in the sedimentary rocks of North America. *Reviews of Geophysics*, *27*(4), 471–494. https://doi.org/10.1029/RG027i004p00471

McFadden, P. L., & Jones, D. L. (1981). The fold test in palaeomagnetism. *Geophysical Journal of the Royal Astronomical Society*, *67*(1), 53–58. https://doi.org/10.1111/j.1365-246X.1981.tb02731.x

Michard, A., Ibouh, H., & Charriére, A. (2011). Syncline-topped anticlinal ridges from the High Atlas: A Moroccan conundrum, and inspiring structures from the Syrian Arc, Israel. *Terra Nova*, *23*(5), 314–323. https://doi.org/10.1111/j.1365-3121.2011.01016.x

Michard, A., Saddiqi, O., Chalouan, A., & Frizon de Lamotte, D. (Eds) (2008). *Continental evolution: The geology of Morocco. Structure, stratigraphy, and tectonics of the African-Atlantic-Mediterranean triple junction*, (Vol. 116). Berlin Heidelberg: Lecture Notes in Earth Sciences.

Missenard, Y. (2006). Le relief des atlas marocains: contribution des processus asthénosphériques et du raccourcissement crustal, Aspects chronologiques. PhD Thesis, University Cergy Pontoise.

Moussaid, B., Villalaín, J. J., Casas-Sainz, A., El Ouardi, H., Oliva-Urcia, B., Soto, R., et al. (2015). Primary vs. secondary curved fold axes: Deciphering the origin of the Aït Attab syncline (Moroccan High Atlas) using paleomagnetic data. *Journal of Structural Geoloy.*, *70*, 65–77. https://doi.org/10.1016/j.jsg.2014.11.004

Piqué, A., Charroud, M., Laville, E., Aït Brahim, L., & Amrhar, M. (2000). The Tethys southern margin in Morocco; Mesozoic and Cainozoic evolution of the Atlas domain. *Mémoires du Muséum National d'Histoire Naturelle*, *182*, 93–106.

Quiquerez, A., Sarih, S., Allemand, P., & García, J. P. (2013). Fault rate controls on carbonate gravity-flow deposits of the Liassic Central High Atlas (Morocco). *Marine and Petroleum Geology*, *43*, 349–369. https://doi.org/10.1016/j.marpetgeo.2013.01.002

Saura, E., Vergés, J., Martín-Martín, J. D., Messager, G., Moragas, M., Razin, P., et al. (2014). Syn- to post-rift diapirism and minibasins of the Central High Atlas (Morocco): The changing face of a mountain belt. *Journal of the Geological Society (London)*, *171*(1), 97–105. https://doi.org/10.1144/jgs2013-079

Scotese, C. R., & Van der Voo, R. (1983). Paleomagnetic dating of Alleghenian folding (abstract). *EOS Transactions of the American Geophysics Union*, *64*, 218.

Shipunov, S. V. (1997). Synfolding magnetization: Detection, testing and geological applications. *Geophysical Journal International*, *130*(2), 405–410. https://doi.org/10.1111/j.1365-246X.1997.tb05656.x

Sibuet, J.-C., Rouzo, S., & Srivastava, S. (2012). Plate tectonic reconstructions and paleogeographic maps of the central and North Atlantic oceans. *Canadian Journal of Earth Sciences*, *49*(12), 1395–1415. https://doi.org/10.1139/e2012-071

Soto, R., Casas-Sainz, A. M., & Villalaín, J. J. (2011). Widespread Cretaceous inversion event in northern Spain; evidence from subsurface and Paleomagnetic data. *Journal of the Geological Society (London)*, *168*(4), 899–912. https://doi.org/10.1144/0016-76492010-072

Soto, R., Casas-Sainz, A. M., Villalaín, J. J., Gil-Imaz, A., Fernández-González, G., del Río, P., et al. (2008). Characterizing the Mesozoic extension direction in the northern Iberian plate margin by anisotropy of magnetic susceptibility (AMS). *Journal of the Geological Society (London)*, *165*(6), 1007–1018. https://doi.org/10.1144/0016-76492007-163

Studer, M., & Du Dresnay, R. (1980). Déformations synsédimentaires en compression pendant le Lias supérieur et le Dogger, au Tizi n'Irhil (Haut Atlas central de Midelt, Maroc). *Bulletin de la Société géologique de France*, *7*(3), 391–397.

Teixell, A., Arboleya, M. L., Julivert, M., & Charroud, M. (2003). Tectonic shortening and topography in the Central High Atlas (Morocco). *Tectonics*, *22*(5), 1051. https://doi.org/10.1029/2002TC001460

Teixell, A., Barnolas, A., Rosales, I., & Arboleya, M. L. (2017). Structural and facies architecture of a diapir-related carbonate minibasin (lower and middle Jurassic, High Atlas, Morocco). *Marine and Petroleum Geology*, *81*, 334–360. https://doi.org/10.1016/j.marpetgeo.2017.01.003

Torres-López, S., Casas, A. M., Villalaín, J. J., El Ouardi, H., & Moussaid, B. (2016). Pre- Cenomanian vs. Cenozoic folding in the High Atlas revealed by palaeomagnetic data. *Terra Nova*, *28*(2), 110–119. https://doi.org/10.1111/ter.12197

Torres-López, S., Villalaín, J. J., Casas, A. M., EL Ouardi, H., Moussaid, B., & Ruiz-Martínez, V. C. (2014). Widespread Cretaceous secondary magnetization in the High Atlas (Morocco). A common origin for the Cretaceous remagnetizations in the western Tethys? *Journal of the Geological Society (London)*, *171*, 673–e687. https://doi.org/10.1144/jgs2013-107

Torsvik, T. H., Van der Voo, R., Preeden, U., Niocaill, C. M., Steinberger, B., Doubrovine, P. V., et al. (2012). Phanerozoic polar wander, palaeogeography and dynamics. *Earth Science Reviews*, *114*(3-4), 195–217. https://doi.org/10.1016/j.earscirev.2012.06.002

Villalaín, J., Fernández-González, G., Casas, A. M., & Gil-Imaz, A. (2003). Evidence of a cretaceous remagnetization in the Cameros basin (North Spain): Implications for basin geometry. *Tectonophysics*, *377*(1-2), 101–117. https://doi.org/10.1016/j.tecto.2003.08.024

Villalaín, J. J., Casas-Sainz, A. M., & Soto, R. (2016). Reconstruction of inverted sedimentary basins from syn-tectonic remagnetizations. A methodological proposal. *Journal of the Geolological Society of London. Special Publication.*, *425*(1), 233–246. https://doi.org/10.1144/SP425.10

Waldhör, M., & Appel, E. (2006). Intersections of remanence small circles: New tools to improve data processing and interpretation in palaeomagnetism. *Geophysical Journal International*, *166*(1), 33–45. https://doi.org/10.1111/j.1365-246X.2006.02898.x

Wilmsen, M., & Neuweiler, F. (2008). Biosedimentology of the Early Jurassic postextinction carbonate depositional system, Central High Atlas rift basin, Morocco. *Sedimentology*, *55*(4), 773–807.

Woods, S. D., Elmore, R. D., & Engel, M. H. (2000). The occurrence of pervasive chemical remanent magnetizations in sedimentary basins: Implications for dating burial diagenetic events. *Journal of Geochemical Exploration*, *69-70*, 381–385. https://doi.org/10.1016/S0375-6742(00)00080-7

Woods, S. D., Elmore, R. D., & Engel, M. H. (2002). Paleomagnetic dating of the smectite-to-illite conversion: Testing the hypothesis in Jurassic sedimentary rocks, Skye, Scotland. *Journal of Geophysical Research*, *107*(B5), 2091. https://doi.org/10.1029/2000JB000053

Zayane, R., Essaifi, A., Maury, R. C., Piqu, E. A., Laville, E., & Bouabdelli, M. (2002). Cristallisation fractionnée et contamination crustale dans la série magmatique jurassique transitionnelle du Haut Atlas central (Maroc). *Comptes Rendus Geoscience. Paris*, *334*(2), 97–104. https://doi.org/10.1016/S1631-0713(02)01716-9